https://doi.org/10.5194/tc-2019-187
Preprint. Discussion started: 10 September 2019

The Cryosphere Discussions

Multi-physics ensemble snow modelling in the western Himalaya

David M. W. Pritchard[1], Nathan Forsythe[1], Greg O'Donnell[1], Hayley J. Fowler[1], Nick Rutter[2]

[1]School of Engineering, Newcastle University, Newcastle upon Tyne, NE1 7RU, United Kingdom
[2]Department of Geography and Environmental Sciences, Northumbria University, Newcastle upon Tyne, NE1 8ST, United Kingdom

Correspondence to: David M.W. Pritchard (david.pritchard@newcastle.ac.uk)

Abstract. Combining multiple data sources with multi-physics simulation frameworks offers new potential to extend snow model inter-comparison efforts to the Himalaya. This study evaluates the importance and performance of different snowpack process representations for simulating snow cover and runoff dynamics in the region. Focusing on the Astore catchment in the upper Indus basin, a spatially distributed version of the Factorial Snowpack Model (FSM) was driven by climate fields from the High Asia Refined Analysis (HAR) dynamical downscaling product. Ensemble performance was evaluated using observed runoff and MODIS remote sensing of snow-covered area, albedo and land surface temperature. The results show that FSM ensemble spread depends primarily on the interactions between parameterisations of albedo and snowpack hydrology when applied in the western Himalaya. These interactions incur variation in the importance of other model choices, most notably the atmospheric stability adjustment. Although no single FSM configuration performs best in all years, applying the prognostic albedo parameterisation while accounting for liquid water retention, refreezing and drainage leads to the highest overall performance. Years when this is not the case tend to coincide with probable inaccuracies in HAR climate inputs. While the results indicate that ensemble spread and errors may be notably lower in anomaly space, FSM configurations show substantial differences in their absolute sensitivity to climate variation. Therefore, a subset of the ensemble should be retained for climate change projections, namely those members including both prognostic albedo and snowpack hydrology, while additional stability adjustment options should be tested.

1 Introduction

Snow plays a profound role in the climate system and supports water resources in many regions (Barnett et al., 2005; Hall and Qu, 2006). As such, several applications depend on process-based models that approximate snow physics while solving mass and energy balances. These include coupled land-atmosphere modelling, testing hypotheses about physical snow processes and catchment behaviour, and hydrological projections in non-stationary climates. Given the number of snow models in existence (e.g. Essery et al., 2013), understanding the relative skill of different models and their suitability for various uses is essential. This is reflected by the succession of snow model inter-comparison initiatives over recent decades (Essery et al., 2009; Etchevers et al., 2004; Krinner et al., 2018; Slater et al., 2001).

https://doi.org/10.5194/tc-2019-187
Preprint. Discussion started: 10 September 2019

While snow models have been evaluated in various contexts, there has been little analysis of how different models perform in the Himalayan region. Yet, vast populations downstream of these water towers are vulnerable to climate change impacts on snowmelt-derived river flows (Bookhagen and Burbank, 2010; Immerzeel et al., 2010; Viviroli et al., 2011). Process-based snow model analysis and inter-comparison in the region would ultimately help to manage these risks, but model input and evaluation is severely impeded by data paucity. Indeed, deriving consistent, multivariate climate input fields in largely unobserved and highly variable mountain environments is a longstanding problem (Klemeš, 1990; Raleigh et al., 2015, 2016). In part this explains the proliferation of simple snow modelling in the region, namely through (sometimes enhanced) temperature index methods (e.g. Lutz et al., 2014; Ragettli et al., 2015; Stigter et al., 2017). There is a small but growing number of offline process-based, energy balance model applications (i.e. not coupled to an atmospheric model), but these have focused only on single model structures, without detailed snow process evaluation (e.g. Brown et al., 2014; Prasch et al., 2013; Shakoor and Ejaz, 2019; Shrestha et al., 2015).

In the face of these data challenges, developments in high resolution regional climate modelling and remote sensing increasingly offer partial solutions. Several studies have now successfully used dynamical downscaling to provide offline forcing for cryospheric and hydrological models in the Himalaya and other contexts (e.g. Biskop et al., 2016; Havens et al., 2019; Huintjes et al., 2015; Tarasova et al., 2016). Similarly, the potential for remote sensing to support model evaluation by providing some constraints on both snow cover dynamics and the surface energy balance has been demonstrated (Collier et al., 2013, 2015; Essery, 2013; Finger et al., 2011). Yet, studies combining these data sources for process-based snow model applications are still few in number (see e.g. Quéno et al., 2016; Revuelto et al., 2018), especially in the Himalaya. Moreover, there has been little examination of how such approaches could support snow model inter-comparison for practical uses, such as water resources modelling and management. This reflects the emphasis of previous inter-comparisons on small scales, such that more systematic studies at larger scales with application-relevant datasets are needed (Essery et al., 2009; Krinner et al., 2018).

Although recent data advances are significant, identifying appropriate model formulations remains challenging even in well-instrumented contexts. In the SnowMIP and SnowMIP2 inter-comparison studies, no single model emerged as optimal, with performance varying between locations and years (Essery et al., 2009; Etchevers et al., 2004; Rutter et al., 2009). Similarly, recent inter-comparisons using more systematic ensemble frameworks have found there to be only groups of model configurations that tend to perform consistently well, poorly or variably (Essery et al., 2013; Lafaysse et al., 2017; Magnusson et al., 2015). Model complexity does not appear to be strongly (or necessarily positively) related to skill or transferability in space and time (see also Lute and Luce, 2017). Nevertheless, the systematic frameworks underpinning recent inter-comparisons are an important advance over earlier studies. By synthesising the array of models in existence and eliminating implementation differences, these frameworks permit better quantification of the behaviour of different parameterisations and identification of where improvements may be possible (Clark et al., 2015; Krinner et al., 2018). The full potential of this approach has not yet been realised, especially in data-sparse mountain regions.

https://doi.org/10.5194/tc-2019-187
Preprint. Discussion started: 10 September 2019

Therefore, this study uses recent progress in high resolution regional climate modelling, remote sensing and ensemble-based snow modelling to assess the performance and behaviour of snowpack model formulations in a western Himalayan catchment. To do this, the High Asia Refined Analysis (HAR, Maussion et al., 2014) dynamical downscaling product is used to drive the Factorial Snowpack Model (FSM) multi-physics ensemble (Essery, 2015). The spatially distributed, high resolution FSM simulations are evaluated using a combination of local observations and multiple MODIS remote sensing products. The aim is to characterise how model performance varies between formulations and in time, while also identifying possible causes and implications of performance variation in simulating snow cover dynamics and snowpack runoff. This contributes to the need for more application-oriented model evaluations using unified frameworks (Clark et al., 2015; Essery et al., 2013), in a context where accurately simulating snow processes is essential for understanding cryospheric, hydrological and water resources trajectories in a changing climate.

2 Study Area

The study focuses on the steep, mountainous Astore catchment, a 3988 km^2 gauged sub-basin of the upper Indus basin (Figure 1). The mean elevation of the catchment is around 4000 mASL, with 57% and 87% of the area lying in the elevation ranges 3500–4500 and 3000–5000 mASL, respectively. River flows are typically very low in winter, before rising in spring and peaking in summer (June/July). Spring/summer runoff is dominated by snowmelt, which is derived primarily from orographically enhanced snowfall in the preceding winter and early spring (Archer, 2003). Much of this snowfall originates from synoptic scale low pressure systems known as westerly disturbances; monsoon influences are small compared with the central Himalaya. Showing notable spatial correlation at the seasonal scale, winter precipitation observations can predict summer runoff totals reasonably for forecasting purposes (Archer and Fowler, 2004; Archer, 2003; Fowler and Archer, 2005). Together with the fact that glacier cover is relatively limited, at around 6% according to the Randolph Glacier Inventory (RGI) 5.0 (Arendt et al., 2015), this indicates that catchment runoff is primarily mass- rather than energy-limited. However, energy constraints certainly affect intra-seasonal variability. The ESA GlobCover 2009 product (Arino et al., 2012) confirms that vegetation cover is relatively sparse, with the catchment dominated by a mixture of bare ground, herbaceous plants, and perennial snow and ice.

3 Data and Methods

3.1 Model

3.1.1 Factorial Snowpack Model (FSM) Overview

FSM is an intermediate complexity, systematic framework for evaluating alternative representations of snowpack processes and their interactions (Essery, 2015). Constructed around a coupled mass and energy balance scheme, FSM was originally formulated as a one-dimensional column model with up to three layers, depending on the total snow depth. The

https://doi.org/10.5194/tc-2019-187
Preprint. Discussion started: 10 September 2019

model is based around the sequential solution of a set of linearised equations at each time step. This begins with the surface energy balance, in which turbulent heat fluxes are estimated using the bulk aerodynamic approach. Heat conduction between layers and to the substrate is calculated using an implicit scheme, before layer ice and water masses are updated to account for simulated rainfall, melt, sublimation, refreezing, drainage to successive layers, and runoff from the base of the snowpack. FSM then updates layer densities and thicknesses, accounting for snowfall and conservation of total ice and liquid water masses, as well as internal energy.

Within this framework, FSM offers alternative parameterisations of different snowpack processes. The five processes are: (1) albedo evolution, (2) thermal conductivity variation, (3) snow density change by compaction, (4) adjustment of turbulent heat fluxes for atmospheric stability, and (5) liquid water retention, refreezing and drainage. With two parameterisation options (0/1) for these five processes, the FSM ensemble includes 32 possible model configurations. Summarised in Table 1, the parameterisation options synthesise a number of approaches found in a range of widely applied models. These include CLASS (Verseghy, 1991), CLM (Oleson et al., 2013), Crocus (Vionnet et al., 2012), HTESSEL (Dutra et al., 2010), ISBA (Douville et al., 1995), JULES (Best et al., 2011), MOSES (Cox et al., 1999) and Noah-MP (Niu et al., 2011). For each process, the second option (1) may be considered more physically realistic than the first option (0).

Analyses of FSM to date have shown that it gives ensemble performance and spread comparable to larger multi-model ensembles (Essery, 2015). As such, it has been used to support study design and inter-comparison in the ESM-SnowMIP initiative (Krinner et al., 2018). Its value for testing new process representations in forest environments has also been demonstrated (Moeser et al., 2016), while Günther et al. (2019) used FSM to delineate the influences of input data errors, model structure and parameter values on simulation performance at an Alpine site.

3.1.2 Adaptations and Implementation

While the core FSM subroutines used in this study remain as described in Essery (2015), the model was adapted to perform spatially distributed simulations on a regular grid, using climate inputs that vary in space and time. In this adaptation, each grid cell is treated as independent of all other cells. Inter-cell mass and energy transfers are not considered, but the default parameterisation of sub-grid variability of snow cover as a function of snow depth is retained. In effect, each grid cell is considered as a site for which the original FSM formulation is run. The adapted version of the model is thus similar in principle to other widely applied, distributed snow models when used without their snow transport options (e.g. Lehning et al., 2006; Liston and Elder, 2006a). In line with the focus on snow cover dynamics and snowpack processes, the model does not simulate other aspects of catchment hydrology, such as evapotranspiration from snow-free cells, the soil water balance, or hydrological routing (subsurface, overland and channel flows).

The simulations reported here use a 500 m horizontal resolution grid and an hourly time step. Topography is derived from the SRTM 90 m DEM v4.1 (Jarvis et al., 2008). The 500 m spatial resolution is representative of hydrological and cryospheric modelling applications in the large basins of the Himalaya (e.g. Lutz et al., 2016), as well as extremely high resolution regional climate modelling (Bonekamp et al., 2018; Collier and Immerzeel, 2015). It is also consistent with

https://doi.org/10.5194/tc-2019-187
Preprint. Discussion started: 10 September 2019

several of the MODIS products used for evaluation (Section 3.3). Spatial variation in land surface properties is ignored on the basis that glacier and vegetation (including forest) cover is low (Section 2) and information on substrate properties is unavailable. The simulations use the default FSM model parameters, which have been shown to reproduce much of the spread in previous model inter-comparisons (Essery, 2015).

3.2 Climate Inputs

3.2.1 High Asia Refined Analysis (HAR)

Spatiotemporally varying input fields of rainfall, snowfall, air temperature, relative humidity, wind speed, surface air pressure, and incoming shortwave and longwave radiation are based on the HAR (Maussion et al., 2014). The HAR is a 14-year dynamical downscaling of coarser global analysis to 10 km over the Himalaya and Tibetan Plateau using the Weather Research and Forecasting model (WRF, Skamarock et al., 2008). Although a seasonally varying cold bias is present in the upper Indus basin, the HAR shows substantial performance in capturing many spatial and temporal patterns in the near-surface climatology (Maussion et al., 2014; Pritchard et al., 2019). The HAR has also exhibited a good representation of climate in several hydrological and glaciological modelling studies in neighbouring regions (Biskop et al., 2016; Huintjes et al., 2015; Tarasova et al., 2016).

3.2.2 Bias Correction and Downscaling

Near-surface air temperature fields were bias-corrected to reduce the HAR's cold bias in the study area. The mean bias was estimated using quality-controlled local observations from stations in the Astore catchment (Figure 1b), which are maintained by the Pakistan Meteorological Department (PMD) and the Water and Power Development Authority (WAPDA). More advanced bias correction approaches were tested, including quantile-based methods, but these did not lead to improvements either in cross-validation at station locations or model performance at the catchment scale. This is likely due to the difficulty of fully characterising spatial and temporal variation in biases based on limited observations, especially for less commonly measured variables. The minimal approach taken thus represents a realistic application. It also has the advantage of retaining much of the physical consistency of the HAR fields in terms of both inter-variable and spatiotemporal dependence structures.

Spatial disaggregation of the 10 km HAR fields to the 500 m FSM grid was conducted using methods adapted from the MicroMet meteorological pre-processor of SnowModel (Liston and Elder, 2006b), as well as the approaches used by Duethmann et al. (2013). For temperature, specific humidity, incoming longwave radiation, pressure and (log-transformed) precipitation, linear regression was used each time step to relate each variable to elevation. If the gradient term in the regression was significant at the 95% confidence level, the values at each HAR cell (10 km grid) were interpolated to a reference level using the gradient. This spatial (horizontal) anomaly field was then interpolated to the high resolution FSM grid (500 m), and the elevation signal was subsequently reintroduced using the regression gradient. Where the gradient term

https://doi.org/10.5194/tc-2019-187
Preprint. Discussion started: 10 September 2019

in the regression was not statistically significant, simple interpolation of the HAR field to the FSM grid was undertaken. Wind speed was interpolated and modulated by topographic slope and curvature using MicroMet.

Due to the pronounced topography of the study area, clear-sky shortwave radiation at the surface was estimated for the 500 m resolution DEM using a vectorial algebra approach (Corripio, 2003). This approach accounts for the effects of slope, aspect, hill-shading and sky view factor. It has been successfully applied before in this region (e.g. Ragettli et al., 2013) and was additionally checked against station measurements. To account for cloud cover, the clear-sky shortwave radiation fields were adjusted using spatially interpolated ratios of clear-sky to received incoming shortwave radiation at the surface according to the HAR. This approach maintains consistency between variables while capturing topographic influences, although direct/diffuse partitioning and cloud variability are simplified.

3.2.3 Uncertainty

Given the low density of climate observations, biases and other errors undoubtedly remain in the climate input fields. As such, two alternative input strategies were tested. The first strategy uses the same approach outlined in Section 3.2.2 but simply forgoes bias correction of temperature. The second strategy retains the same approaches for precipitation, incoming shortwave radiation and wind speed, but local observations from the Astore and other catchments in the north-west upper Indus basin (Figure 1b) are used as the basis for estimation of fields for the other variables (see Section S1 in Supplement). The purpose of these two alternative strategies is to indicate whether the conclusions reached on snowpack process representations are unduly affected by the approaches described in Section 3.2.2.

3.3 Model Evaluation

The model evaluation focuses primarily on snow cover and snowpack runoff, with other variables considered to evaluate underlying processes. Typical of the remote Himalaya, no local snow measurements for site-scale evaluation were available. The evaluation thus uses a number of MODIS remote sensing products (Collection 6). These include snow-covered area (SCA) derived from the MOD10A1 product (Hall and Riggs, 2016), following application of the widely used cloud infilling method developed by Gafurov and Bárdossy (2009). The analysis focuses primarily on SCA corresponding with a Normalised Difference Snow Index (NDSI) threshold of zero. This indicates very limited or no snow cover in a pixel (Salomonson and Appel, 2004), which is consistent with the no-snow threshold used to estimate modelled SCA.

The evaluation also draws on the MCD43A3 and MOD10A1 surface albedo products. These datasets have been validated in different settings (Gascoin et al., 2017; Liu et al., 2009; Wang et al., 2012), but additional challenges are posed by complex terrain (Wen et al., 2018). The evaluation thus considers the model results and datasets in both absolute and normalised terms. In addition, comparisons with MOD11A1 land surface temperature (LST) are undertaken. To extend previous validations (e.g. Wan, 2014; Wan et al., 2004), an evaluation of MOD11A1 at the Concordia site (Figure 1b) in the neighbouring Karakoram range is given in the Supplement (Section S2). This confirms that the product performs well

https://doi.org/10.5194/tc-2019-187
Preprint. Discussion started: 10 September 2019

compared with observed surface temperatures, with a relatively low mean bias of -0.55°C. For both albedo and LST, spatial aggregates were only calculated when 90% of pixels had satisfactory quality retrievals.

The study also uses quality-controlled daily river flows recorded at the Doyian gauging station by WAPDA (Figure 1b). These data allow for some inferences about the volume and timing of modelled snowpack runoff, which is defined here as runoff from the base of the snowpack. Snowpack runoff is thus different to surface melt, which may be subject to storage and refreezing processes before leaving the snowpack. Snowpack runoff is aggregated across all grid cells in the catchment for comparison with the observed data.

4 Results

4.1 Mean Ensemble Structure

4.1.1 Snowpack Runoff

The evaluation begins by considering how the FSM ensemble is structured on average at the catchment scale. For snowpack runoff (as defined in Section 3.3), the ensemble shows notable spread, which takes the form of groupings of ensemble members (Figure 2). Three groups of cumulative snowpack runoff curves are distinguishable early in the melt season (April and early-May) in Figure 2, but the groups split and their spread increases to varying degrees thereafter, as melt rates accelerate. Differences in snowpack runoff timing between groups are substantial, with variation of around one month in the date at which the 25^{th}, 50^{th} and 75^{th} percentiles of total seasonal runoff are exceeded.

Figure 2a indicates that the development of groups in the ensemble is primarily controlled by interactions between parameterisations of albedo and liquid water processes within the snowpack. The earliest, most rapid snowpack runoff occurs for members combining diagnostic albedo with instantaneous liquid water drainage (grey in Figure 2a). In contrast, the slowest-responding members (purple in Figure 2a) use prognostic albedo and apply the parameterisation of liquid water retention, refreezing and drainage processes (hereafter referred to as the liquid water parameterisation). The remaining two combinations of albedo and liquid water representations result in similar cumulative runoff curves, especially early in the season (orange and green in Figure 2a). This indicates that a propensity for earlier, more rapid runoff when applying diagnostic albedo is offset by a delaying effect of the liquid water parameterisation. Conversely, a tendency delaying runoff in the prognostic albedo parameterisation is counteracted by faster runoff due to instantaneous drainage. Interactions between the albedo and liquid water parameterisations thus appear to govern whether a given option's tendency to accelerate or slow snowpack runoff is compensated for or exacerbated.

The next most important determinant of ensemble structure for snowpack runoff is the stability adjustment option, whose significance increases later in the melt season, especially in July. As noted above, Figure 2a indicates that the spread in the ensemble groups increases with time. Cross-referencing this with Figure 2b confirms that the stability adjustment is the main driver of the divergence. The separation is particularly pronounced for the slowest-responding ensemble members

https://doi.org/10.5194/tc-2019-187
Preprint. Discussion started: 10 September 2019

(purple in Figure 2a). In this case, not applying a stability adjustment leads to more rapid snowpack runoff from mid-June and earlier convergence with the other ensemble members, as evident from comparing the lowermost orange and blue curves in Figure 2b. In contrast, the adjustment effect is much less pronounced for the faster-responding groups of ensemble members in Figure 2a (grey curves). Therefore, not only does the significance of the stability adjustment vary notably through the melt season, it is also a function of the choices of albedo and liquid water parameterisations.

Figure 2a also provides a preliminary indication that the timing of snowpack runoff in the slowest-responding ensemble members, which combine prognostic albedo with the liquid water parameterisation, is most similar to the timing of observed catchment runoff on average. This can be inferred particularly from the snowmelt-dominated early part of the season (April, May and early June), when the other groups of ensemble members tend to lead the observed total runoff curve by between two and four weeks. While the full hydrology of the Astore catchment is not modelled (Section 3.1.2), such large differences in timing are unlikely to be accounted for by runoff routing or other hydrological processes at this time of year. Based on findings from snow-dominated mountainous catchments elsewhere and other settings, runoff travel times from the base of the snowpack to the catchment outlet in spring and early summer are expected to be small relative to the ensemble spread in Figure 2a, even in a catchment of this size (Lundquist et al., 2005; Naden, 1992).

4.1.2 Snow-Covered Area (SCA)

Figure 3 indicates that the albedo, liquid water and stability adjustment parameterisations are also the main influences on mean ensemble spread and structure in SCA. However, the dominance of albedo and liquid water processes is lesser compared with snowpack runoff, especially later in the melt season. By the annual SCA minimum in August, the stability adjustment comes to control ensemble structure (Figure 3b). Model configurations applying the adjustment exhibit a markedly slower decline in SCA over the melt season, which leads to an annual SCA minimum approximately 5% higher. Spatially, this difference is largely found at relatively high elevations, which could have substantial implications for modelling the evolution of ice mass in the catchment over longer periods.

For much of the melt season, the model configurations most closely matching MODIS SCA (using an NDSI threshold of zero – see Section 3.3) apply prognostic albedo, along with either no liquid water representation but a stability adjustment, or the liquid water parameterisation but no stability adjustment. Again this reflects compensatory effects in the ensemble. Switching on the liquid water representation slows the rate of SCA decline, while turning off the stability adjustment speeds it up, and vice versa. For most of the other ensemble members, the SCA curves exhibit a relatively rapid snow cover decline during the melt season compared with MODIS (NDSI threshold of zero).

Comparing Figure 2 and Figure 3 suggests that model configurations where snowpack runoff is closer to observed total runoff also agree better with MODIS SCA, although this is complicated by the larger spread in ensemble groups for SCA. The clearest case is for ensemble members that both apply diagnostic albedo and omit a liquid water representation. These configurations show snowpack runoff that appears to be too early and rapid (Figure 2a), as well as too fast a decline in SCA (Figure 3a). The other combinations of albedo and liquid water parameterisations perform better for both variables overall,

https://doi.org/10.5194/tc-2019-187
Preprint. Discussion started: 10 September 2019

but this does depend substantially on the stability adjustment for SCA. Notably, the slowest-responding model configurations (using prognostic albedo, the liquid water parameterisation and the stability adjustment) are too slow in their SCA decline from June onwards (Figure 3). This may well highlight too slow a response in snowpack runoff later in the melt season that is ambiguous from Figure 2 alone, which highlights the value of MODIS SCA for reinforcing and extending inferences on model configuration performance (Finger et al., 2011).

4.2 Process Evaluation

The analysis now explores the processes behind the structure of ensemble spread identified in Section 4.1, as well as how far they can be assessed with independent data. This assessment is based in part on Table 2, which summarises the mean influences of albedo, liquid water and stability adjustment parameterisation choices on key catchment-scale states and fluxes in selected months. The influences are delineated as the monthly mean differences between those ensemble members applying one option for a given process (e.g. prognostic albedo) and those members applying the other option (e.g. diagnostic albedo). Density and thermal conductivity parameterisations are not considered, as it can be inferred from Section 4.1 that their effects are comparatively minor for the foci of this study, namely runoff and SCA.

4.2.1 Albedo

Table 2 shows that prognostic albedo in FSM tends to be higher than diagnostic albedo in the first part of the melt season. The mean difference between the two albedo options ranges from 0.12 to 0.15 between April and June at solar noon. The resulting difference in net shortwave radiation helps to explain why prognostic albedo initially delays and slows melt, snowpack runoff and SCA decline relative to diagnostic albedo, which ultimately permits more snowpack runoff later in the season (see Section 4.1 and Table 2). One factor in the faster melt in spring and early summer using diagnostic albedo is its pronounced diurnal range. This is linked to the diurnal surface temperature cycle, partly through a positive feedback. The mean range in albedo for daylight hours rises from 0.18 to 0.27 between April and June when using the diagnostic parameterisation, whereas the equivalent range for the prognostic parameterisation stays much lower, at around 0.02. While albedo does vary diurnally with solar zenith angle, it does not necessarily follow that the diagnostic parameterisation captures the magnitude of variation appropriately.

In absolute terms, FSM mean snow albedo from March to August exceeds MODIS by 0.07 and 0.14 for MOD10A1 and MCD43A3, respectively. This may be in part due to challenges in fully characterising albedo in complex terrain with remote sensing (Wen et al., 2018). However, after normalising to remove differences in the mean, Figure 4 demonstrates that the prognostic albedo parameterisation is in reasonable agreement with MODIS. Acknowledging some timing offsets and points of divergence between the MODIS products, prognostic albedo more skilfully captures the sharp albedo increases following snowfall in the melt season. Field studies have shown these events to be an important for regional melt rate variability, especially early in the season, in accordance with the latitude (~35°N) and continentality of the area (Hewitt, 2014). The prognostic parameterisation also generally reproduces the rate of albedo decay during melting periods in Figure 4, whereas

https://doi.org/10.5194/tc-2019-187
Preprint. Discussion started: 10 September 2019

the diagnostic parameterisation induces frequent, sharp and pronounced albedo fluctuations. These fluctuations give rise to a comparatively low albedo in the early melt season. In quantitative terms, the prognostic parameterisation outperforms the diagnostic option for the normalised series, with an overall root-mean-square deviation (RMSD) relative to the MOD10A1 product of 0.062 compared with 0.071. Process-level evaluation with MODIS thus corroborates the better performance of prognostic albedo for simulating snowpack runoff and SCA (Section 4.1).

4.2.2 Liquid Water Retention, Refreezing and Drainage

Table 2 shows that the net effect of switching on the liquid water parameterisation is to delay snowpack runoff, even though it accelerates surface melt rates. For example, in April (May), snowpack runoff is on average 1.9 (1.6) mm/d lower when using the liquid water parameterisation, even though surface melt is 1.0 (1.9) mm/d higher. With the option on, liquid water from melting is allowed to refreeze, leading to latent heat release, which maintains a higher snowpack temperature (for example by 3.5°C in April). Retention and delayed release of liquid water in storage are part of the reason why these higher temperatures lead to higher melt rates but not higher snowpack runoff rates initially. However, multiple diurnal cycles of melting and refreezing may also be required before a given unit of snow is entirely converted to snowpack runoff. At any rate, the delaying effect of switching on the liquid water option outweighs its tendency to increase melt rates in this setting. By allowing snow to persist for longer, this enhanced storage ultimately leads to higher melt and runoff rates later in the season (by July), as later-lying snow becomes subject to increasing energy inputs (e.g. Musselman et al., 2017).

4.2.3 Stability Adjustment

Table 2 also demonstrates that switching on the stability adjustment leads to lower melt rates later in the season, primarily due to a smaller sensible heat flux towards the snow surface in stable atmospheric conditions. During the early part of the season (e.g. April), the differences in net turbulent fluxes arising from the stability adjustment choice (16 W/m^2) are largely offset by differences in net radiation (12.3 W/m^2). The larger sensible heat flux to the surface with no stability adjustment leads to a higher surface temperature (by 2.9°C in April) and thus higher outgoing longwave radiation, as well as lower net longwave radiation. However, as the gradients between the snow surface (limited to 0°C) and near-surface air temperatures increase in spring and summer, the net turbulent flux difference ultimately becomes a key driver of differences in the surface energy balance and melt rates. By June and July, the differences in net radiation (16 and 20 W/m^2) no longer offset the differences in net turbulent fluxes (36.8 and 52.7 W/m^2). Yet, Table 2 also indicates that the resulting differences in melt rates do not necessarily alter snowpack runoff on average. This reinforces the point that modelled snowpack runoff sensitivity to the stability adjustment is contingent on the representations of other processes, namely albedo and liquid water retention, refreezing and drainage (Section 4.1.1). It is also noteworthy that switching on the stability adjustment approximately halves average sublimation from 80 to 45 mm/a, which correspond with around 8% and 4% of total catchment snow ablation, respectively.

https://doi.org/10.5194/tc-2019-187
Preprint. Discussion started: 10 September 2019

While no data to evaluate turbulent fluxes directly are available, Figure 5 shows that switching off the stability adjustment leads to higher LST, which is in fact in closer agreement with MODIS LST. This is somewhat counter to initial expectations, as applying a stability adjustment would typically be considered more physically realistic. The largest differences in vertical LST profiles occur at night and increase with elevation, for the clear-sky conditions when MODIS retrievals are available. These differences may suggest too strong a suppression of turbulent fluxes under stable conditions using the bulk Richardson number correction. Such suppression may well contribute to the slow runoff rise and SCA decline when combining the stability adjustment with the otherwise realistic configuration of prognostic albedo and the parameterisation of liquid water processes (Section 4.1). Ensemble spread in day-time LST is smaller and generally in good agreement with MODIS, although the extent and influence of sub-pixel snow cover variation on MODIS LST likely increases during melting periods, giving some positive bias in summer (Section S2 in Supplement).

4.2.4 Vertical Profiles

Figure 6 examines how the tendencies identified above are manifest spatially, as well as how the influence of different processes depends on both space and time. Focusing on the vertical dimension, Figure 6 shows that S-shaped profiles of snowpack runoff differences develop and migrate upwards as the melt season progresses. The profiles take this form because the 0 options in FSM for albedo, liquid water and stability adjustment processes all lead to earlier and faster snowpack runoff and snow water equivalent (SWE) depletion relative to the 1 options (see Table 1). This gives negative differences at higher elevations. However, it also means that the 1 options (i.e. prognostic albedo, liquid water processes represented and stability adjustment applied) are associated with larger SWE later in the season, allowing more snowpack runoff at lower elevations (positive differences in Figure 6). This is consistent with the catchment responses described above, although the inter-annual variation in the magnitude of differences is notable.

The S-shaped profiles migrate upwards in sequence, with the profile for differences due to liquid water processes peaking at the highest elevations, followed by the albedo and stability adjustment profiles. The liquid water option choice is particularly critical around the freezing isotherm for daily maximum temperatures, determining whether early melt is released or subject to storage through refreezing/melting cycles (Section 4.2.2). In comparison, the lower elevation of peak negative differences caused by the albedo parameterisation is likely consistent with a higher snow surface temperature under slightly higher daily mean air temperatures. The peak negative differences due to the stability adjustment option are at lower elevations again, reflecting their dependence on the development of large near-surface temperature gradients (Section 4.2.3). Notably, for both albedo and particularly liquid water processes, differences in snowpack runoff are present up to the highest elevations. Therefore, how these processes are represented is critical for simulating high elevation perennial snow and ice.

https://doi.org/10.5194/tc-2019-187
Preprint. Discussion started: 10 September 2019

4.3 Performance Variation

4.3.1 Absolute Performance and Trade-Offs

The analysis now considers how model performance varies in time with inter-annual climate variations. Figure 7a shows the relationship between RMDS for cumulative snowpack runoff and SCA, with the ensemble aggregated by albedo, liquid water and stability adjustment options. For snowpack runoff, RMSD was calculated for each year based on the cumulative runoff curves for the period between April and June. For each year, the curves were first normalised by (dividing by) their respective total runoff volumes between April and September, in order to focus on differences in timing rather than total volumes. For SCA, RMSD was calculated for the period between April and September using an NDSI threshold of zero for MODIS (see Section 3.3).

Figure 7a confirms that, for individual years as well as on average, ensemble groups exhibiting closer correspondence between snowpack runoff and observed total runoff also tend to show more consistency with MODIS SCA. This provides additional support for the suggestion that snowpack runoff dominates river flows in spring and early summer, with routing effects and other influences being relatively small. Figure 7a also confirms that using both prognostic albedo and the liquid water parameterisation generally leads to the best performance (Section 4.1). However, the group omitting liquid water processes but applying the stability correction also shows low mean RMSD overall, especially for SCA. As Section 4.2.3 strongly suggests the stability adjustment to be too strong in damping turbulent fluxes in stable conditions, it is possible to identify these compensatory effects as unphysical.

Inter-annual variability in RMSD for all groups is high, as reflected by the wide and overlapping error bars in Figure 7a. Although substantial asymmetries and trade-offs between runoff and SCA RMSDs are present, the range of RMSD tends to be smaller for groups performing better on average. However, in some years, configurations tending to perform worse on average may outperform more realistic configurations. To examine this, the relationships between performances of different groups are shown in Figure 7b. Focusing on runoff RMSD for the three best-performing groups overall, Figure 7b shows that trade-offs resembling a Pareto front develop in some cases. This means that, for a number of the years simulated, performance in one group cannot increase without a corresponding reduction in performance of another group. Specifically, there are a number of years in which good performance with the liquid water option off (and the stability adjustment applied) is associated with performance reductions in more physically realistic configurations where the liquid water option is switched on (blue and orange points on Figure 7b).

In other cases, such as when prognostic albedo and the liquid water parameterisation are both applied but the stability adjustment is varied (grey points on Figure 7b), a Pareto-like front is absent and a more linear relationship between runoff RMSDs occurs. This relationship is approximately centred on the 1:1 line in Figure 7b, albeit with notable scatter, most of which is associated with the simulations using observation-based climate inputs, which may be the least accurate input strategy (Section 3.2.3 and Section S1 in the Supplement). This suggests that, overall, model performance limitations are not due to varying the stability adjustment option in this case. Rather, any structural constraint on performance is common to

https://doi.org/10.5194/tc-2019-187
Preprint. Discussion started: 10 September 2019

both configurations, namely through the dominance of the albedo and snowpack hydrology parameterisations and their response to the climate conditions of a particular year. More such inter-group comparisons are provided in the Supplement (Section S3). This shows that a range of linear relationships and Pareto-like fronts – as well as combinations of the two – are present across the full ensemble.

4.3.2 Time Series

To explore further performance variation in time, Figure 8a shows time series of absolute SCA errors (calculated as FSM minus MODIS). This demonstrates that the best-performing group varies both between and within years, but that the structure of the ensemble remains fundamentally similar between years. Specifically, while the groups of FSM configurations all converge in winter, their divergence in spring and summer follows a similar pattern each year. The group using prognostic albedo and the liquid water parameterisation is consistently the uppermost series in Figure 8a, while the group using diagnostic albedo and no liquid water parameterisation is consistently the lowermost. The rank order of the groups remains the same through time, although the magnitude of divergence varies notably between years. In some years, fast-responding combinations (Section 4.1) exhibit the lowest overall errors in at least part of the melt season (for example 2001, 2002, 2005 and 2007). Autumn convergence of groups is often associated with larger SCA errors, due to difficulties capturing specific snowfall and melt events.

Despite these patterns of divergence and variation in absolute errors, Figure 8b indicates that, in anomaly space, the different FSM configurations are generally much more consistent, both with each other and with remote sensing. Anomalies were calculated by subtracting the mean SCA for each month from the absolute SCA, separately for MODIS and the ensemble groups. The sign and magnitude of SCA anomalies are generally well simulated, and the range in anomalies shown in Figure 8b is clearly much smaller than the range of absolute errors during spring and summer in different configurations (Figure 8a). While the focus here is on SCA, as the comparison with MODIS is fairly direct, the consistency of different configurations in anomaly space is also evident for snowpack runoff and LST, as shown in the Supplement (Section S4). With potentially important implications for seasonal forecasting, this reflects the dominance of climatic drivers in shaping the response of diverse snow models.

However, Figure 8b also shows that there are some instances where errors are still large in anomaly space. To explore whether these errors could be due to climate inputs, rather than model response, Figure 8c provides time series of seasonal precipitation and temperature anomalies from the HAR input data product and local observations. As noted in Section 2, local observations show strong spatial correlation at the seasonal scale (Archer and Fowler, 2004; Archer, 2004). While the HAR provides reasonable climatological performance in many respects (Section 3.2.1), Figure 8c suggests that its agreement with observed seasonal climate anomalies is quite variable. Taking the underestimation of the negative SCA anomaly in spring/summer 2001 in Figure 8b as an example (labelled as (i) on Figure 8), Figure 8c indicates that HAR precipitation anomalies in the (preceding) winter and (contemporaneous) spring/summer are reasonable, but that the positive observed temperature anomalies are substantially underestimated by the HAR. The erroneously cool conditions would be conducive to

https://doi.org/10.5194/tc-2019-187
Preprint. Discussion started: 10 September 2019

relatively slow simulated melt rates. This helps to explain the error in anomaly space, as well as the large absolute SCA error in the slower-responding, more physically realistic configurations in Figure 8a (i.e. prognostic albedo with representation of liquid water processes).

Table 3 details more such examples. Together, these cases strongly suggest that the larger discrepancies between modelled and remotely sensed SCA in anomaly space may be related to issues with the sequences of climate (input) anomalies. Importantly, the examples also generally imply that nudging the climate anomalies towards observations would lead to reduction of absolute errors for the more physically realistic configurations, similar to example (i) discussed above. Thus, there is evidence that errors in climate input anomalies are a substantial factor in performance variation for FSM configurations in the Astore catchment, which partly explains poor performance of more realistic models in some years.

4.4 Climate Sensitivity

While simulating specific sequences of climate anomalies and snowpack response is critical for applications such as forecasting, correctly representing the sensitivity of snow processes to climate variations and perturbations is crucial for offline and online climate change projections. Given the limitations in the climate input anomaly sequencing identified in Section 4.3.2, this section makes some inferences about the climate sensitivity of FSM configurations on the basis of inter-annual variability. The focus here is on snowpack runoff in the early part of the melt season (April), when snow is typically abundant, such that runoff is primarily constrained by energy rather than mass availability (Section 2) and dominated by snowmelt (see also Sections 4.1 and 4.3.1).

Figure 9 shows the relationship between simulated 10-day air temperature and snowpack runoff anomalies for the four combinations of albedo and liquid water parameterisations. The equivalent relationship using observed temperatures and total runoff is also shown. Figure 9 indicates that the sensitivity of snowpack runoff to climate (temperature) anomalies varies significantly for different model configurations. While scatter in the relationships are notable, likely reflecting the significant influence of other climate variables on the surface energy balance, the relationships are reasonably well approximated by linear regression (all with positive and statistically significant gradients at the 95% confidence interval). Notably, the shallowest gradient, which is associated with configurations using prognostic albedo and the liquid water parameterisation, agrees best with observations. The consistency of the ranking of the four groups (and observations) can be confirmed with bootstrapping, which shows that 77% of realisations have the same order as in Figure 9 (89-98% of realisations if looking at consecutive groups in terms of pair-wise rankings). While the multivariate relationships between snow model response and other climate variables could be explored, the example in Figure 9 already demonstrates how fundamental and important differences in absolute climate sensitivity can be inferred and assessed from (observable) variability.

https://doi.org/10.5194/tc-2019-187
Preprint. Discussion started: 10 September 2019

5 Discussion

The results in Section 4 confirm that several findings from previous snow model inter-comparisons hold in the western Himalaya. Prognostic albedo and inclusion of snowpack hydrology tend to be associated with the best overall model performance in the Astore catchment, which is similar to findings from the European Alps (Essery et al., 2013; Magnusson et al., 2015). In addition, the results reinforce the importance of interactions between process parameterisations, which leads to contingency of sensitivity estimates for a given process on other aspects of model configuration (Günther et al., 2019; Lafaysse et al., 2017). There is also further evidence here that turbulent heat fluxes can be overly suppressed under stable atmospheric conditions when using a stability adjustment based on the bulk Richardson number (e.g. Andreas, 2002; Collier et al., 2015; Slater et al., 2001), such that testing additional approaches would be valuable (Andreadis et al., 2009; Lapo et al., 2019). The results reflect the consensus from site-based inter-comparisons that no single model configuration performs best in all conditions, but that subsets of typically better-performing models are identifiable (Essery et al., 2013; Lafaysse et al., 2017; Magnusson et al., 2015). Further work could explore whether this is the case elsewhere in the Himalaya and neighbouring ranges, for example in heavily monsoon-influenced areas.

By extending previous site-based inter-comparisons to a western Himalayan catchment, the study demonstrates the potential for combining dynamical downscaling products, remote sensing and local observations to drive, evaluate and constrain process-based ensemble snow models at large, application-relevant scales in data-sparse mountain regions. In doing so, the results suggest that process-based models could ultimately be deployed in more situations in the Himalaya. For example, it would now seem possible to assess whether estimates of the contributions of snowmelt to river flows using temperature index models (e.g. Armstrong et al., 2019) hold when more processes are incorporated. The results also reveal the potential for structural similarity in a systematic snow model ensemble in different years, as well as the hierarchy of process interactions leading to this consistent behaviour. Local climate observations can help to identify when poor performance in more physically realistic model configurations at catchment scales is likely driven by input errors, rather than model response errors. Moreover, using variability as a guide to the climate sensitivity of different model configurations can provide additional confidence when selecting ensemble members for applications like climate change projections. This may have substantial implications for projections of snow dynamics in a warming world, which are associated with important feedbacks at a range of scales (e.g. Musselman et al., 2017; Palazzi et al., 2017; Pepin et al., 2015).

Uncertainty in these results stems largely from input and evaluation data limitations, applying representative parameter values used in previous studies rather than attempting local calibration, and omitting some snow processes. In terms of input data, biases and other errors inevitably limit model performance in such a data-sparse context. However, Section S5 in the Supplement shows that the structure of the ensemble and overall performance variation remain similar when applying two alternative input strategies (Section 3.2.3 and Section S1). Although the distinction of groupings in the ensemble does reduce when using the more observation-based strategy (Figure S5 in the Supplement), this may well be the least accurate approach, due to the small number of stations available for extrapolation. Therefore, the results show some robustness to alternative,

https://doi.org/10.5194/tc-2019-187
Preprint. Discussion started: 10 September 2019

commonly applied methods for deriving climate input fields in mountain regions for practical applications. Further work could attempt a more quantitative uncertainty analysis, but defining meaningful bias ranges and error distributions to test is challenging given currently available local observations.

For parameter values, the FSM defaults appear reasonable for the Astore catchment, based on the overall performance of more physically plausible configurations, as well as process-level evaluation where possible, such as for albedo (Section 4.2.1). Indeed, the results show there to be notable agreement in multiple simulated and observed variables in both absolute and normalised/anomaly terms, which is strengthened by physical consistency between different observed and remotely sensed variables. Further work could undertake calibration and sensitivity analyses, but this would need to guard against overfitting, error compensation and potentially unphysical behaviour given local data limitations, especially for less realistic parameterisations. In any case, recent work suggests that parameter choice may be of lower importance than both input errors and process parameterisations (Günther et al., 2019).

Some omitted snow processes that may be of less importance for studies such as this one, which examines a relatively short period primarily at the catchment scale, could become important in other applications in the Himalaya. These processes could include avalanching, as well as wind redistribution of snow and associated sublimation (e.g. Litt et al., 2019; Stigter et al., 2018). Although initial testing showed the overall results of this study to be relatively insensitive to the SnowSlide avalanching parameterisation (Bernhardt and Schulz, 2010), these processes have been demonstrated to be important at some scales in Alpine contexts (Bernhardt et al., 2012; Musselman et al., 2015; Strasser et al., 2008). Coupling FSM with existing snow redistribution models would be possible (e.g. Lehning et al., 2006; Liston and Elder, 2006a), but ideally such simulations would be driven by higher resolution dynamical downscaling products than the HAR (e.g. Vionnet et al., 2014). For some applications it could also useful to run FSM at higher spatial resolutions (e.g. Baba et al., 2019; Sohrabi et al., 2019; Winstral et al., 2014), although testing showed similar results at both 250 and 1000 m resolutions.

In addition to alternative stability adjustments, further model development could consider terrain enhancement of longwave radiation (Sicart et al., 2006), refined treatment of sub-grid variability (Clark et al., 2011), and sensible and latent heat advection (Harder et al., 2017). Incorporation of these processes could potentially lead to some model performance gains and further insights into additional factors affecting the interplay of radiative fluxes, turbulent fluxes and surface temperatures. However, they would also increase complexity, dimensionality and the likelihood of error compensation.

6 Conclusion

This study demonstrates that combining local observations, dynamical downscaling and remote sensing products with multi-physics ensemble frameworks facilitates the identification of skilful process-based snow model configurations in the western Himalaya. Although the importance of different snowpack processes varies with time, space and other model options, the results show that the structure of the FSM ensemble is similar between years. Different process parameterisations consistently act to accelerate or delay snowpack runoff and SCA decay. In agreement with other studies,

https://doi.org/10.5194/tc-2019-187
Preprint. Discussion started: 10 September 2019

the results indicate that the prognostic albedo parameterisation should be preferred (Essery et al., 2013; Magnusson et al., 2015). Representation of liquid water retention, refreezing and drainage in the snowpack is also generally required, unless compensatory effects are introduced by other aspects of model configuration, especially the atmospheric stability adjustment option. However, there is evidence that turbulent fluxes are overly suppressed in some conditions by applying the adjustment based on the bulk Richardson number implemented in FSM. Correctly simulating these fluxes is a major ongoing challenge in land surface modelling (Lapo et al., 2019).

While no model configuration performs best in all years, there is evidence to suggest that errors in climate input anomalies play a key role in this, not just model structural limitations. Model snow cover dynamics and runoff responses to climate variations are more consistent in anomaly space, which may be useful in forecasting applications, but there is substantial spread within the ensemble in terms of absolute climate sensitivity. This variation in climate sensitivity is critical for model selection in both offline and online simulations supporting climate change impact projections. Together, these points suggest that an ensemble modelling approach should be used in applications where possible. However, a subset of the full FSM ensemble could be taken forward, namely those members which use prognostic albedo and account for snowpack hydrology. Further work could examine input uncertainties in more detail, as well as alternative process parameterisations (especially for the stability adjustment), parameter value sensitivity, and additional unrepresented processes (such as snow redistribution). In the complex terrain of the western Himalaya, these tasks would all benefit from higher resolution dynamical downscaling products. This could ultimately lead to improved modelling tools to support water resources management in the Himalaya and other mountain regions in a changing climate.

7 Code Availability

The open source FSM model code is available here: https://github.com/RichardEssery/FSM. An extended version with additional physics and options for multi-site simulations is found at: https://github.com/RichardEssery/FSM2. The scripts used to prepare climate inputs and conduct spatially distributed simulations can be requested from the corresponding author.

8 Data Availability

The HAR data product is publicly available at this site: http://www.klima-ds.tu-berlin.de/har/. MODIS data are publicly available; instructions for downloading the products used in this study can be obtained from: https://lpdaac.usgs.gov/products/mcd43a3v006/, https://lpdaac.usgs.gov/products/mod11a1v006/, and https://nsidc.org/data/mod10a1. Most of the observed climate and river flow data are not publicly available, but they can be requested from PMD and WAPDA. Tables summarising station metadata and climatology are also available in various publications (e.g. Archer and Fowler, 2004; Archer, 2003; Mukhopadhyay and Khan, 2016; Sharif et al., 2013; Waqas and Athar, 2018). The climate data from the EvK2CNR Concordia site can be downloaded from: http://share.evk2cnr.org/.

https://doi.org/10.5194/tc-2019-187
Preprint. Discussion started: 10 September 2019

9 Author Contributions

With input from NF, GOD, HF and NR, DP designed the study, conducted the modelling and led the analysis. All authors contributed to the interpretation of results. DP drafted the manuscript, with NF, GOD, HF and NR all providing ideas and alterations.

10 Competing Interests

The authors declare that they have no conflict of interest.

11 Acknowledgements

The authors are grateful to PMD, WAPDA and EvK2CNR for the in-situ observations used in this study. We would also sincerely like to thank Fabien Maussion and colleagues for making the HAR dataset publicly available, as well as Richard Essery for making the FSM program open source. During this study Hayley Fowler was funded by the Wolfson Foundation and the Royal Society as a Royal Society Wolfson Research Merit Award (WM140025), as well as the European Research Council Grant, INTENSE (ERC-2013-CoG-617329). Nathan Forsythe was supported by the Royal Society (CH160148 and CHG\R1\170057) and David Pritchard by an EPSRC doctoral training award (EP/M506382/1).

https://doi.org/10.5194/tc-2019-187
Preprint. Discussion started: 10 September 2019

References

Andreadis, K. M., Storck, P. and Lettenmaier, D. P.: Modeling snow accumulation and ablation processes in forested environments, Water Resour. Res., 45, W05429, doi:10.1029/2008WR007042, 2009.

Andreas, E. L.: Parameterizing Scalar Transfer over Snow and Ice: A Review, J. Hydrometeorol., 3, 417–432, doi:10.1175/1525-7541(2002)003<0417:PSTOSA>2.0.CO;2, 2002.

Archer, D.: Contrasting hydrological regimes in the upper Indus Basin, J. Hydrol., 274, 198–210, doi:10.1016/S0022-1694(02)00414-6, 2003.

Archer, D. R.: Hydrological implications of spatial and altitudinal variation in temperature in the Upper Indus Basin, Nord. Hydrol., 35(3), 209–222, doi:10.2166/nh.2004.0015, 2004.

Archer, D. R. and Fowler, H. J.: Spatial and temporal variations in precipitation in the Upper Indus Basin, global teleconnections and hydrological implications, Hydrol. Earth Syst. Sci., 8(1), 47–61, doi:https://doi.org/10.5194/hess-8-47-2004, 2004.

Arendt, A., Bliss, A., Bolch, T., Cogley, J. G., Gardner, A. S., Hagen, J.-O., Hock, R., Huss, M., Kaser, G., Kienholz, C., Pfeffer, W. T., Moholdt, G., Paul, F., Radić, V., Andreassen, L., Bajracharya, S., Barrand, N. E., Berthier, E., Bhambri, R., Brown, I., Burgess, E., Burgess, D., Cawkwell, F., Chinn, T., Copland, L., Davies, B., De Angelis, H., Dolgova, E., Earl, L., Filbert, K., Forester, R., Fountain, A. G., Frey, H., Giffen, B., Guo, W. Q., Gurney, S., Hagg, W., Hall, D., Haritashya, U. K., Hartmann, G., Helm, C., Herreid, S., Kapustin, G., Khromova, T., König, M., Kohler, J., Kriegel, D., Kutuzov, S., Lavrentiev, I., Lebris, R., Nosenko, G., Negrete, A., Nuimura, T., Nuth, C., Pettersson, R., Racoviteanu, A., Ranzi, R., Rastner, P., Rau, F., Raup, B., Rich, J., Rott, H., Sakai, A., Schneider, C., Seliverstov, Y., Sharp, M., Sigurðsson, O., Stokes, C., Way, R. G., Wheate, R., Winsvold, S., Wolken, G., Wyatt, F. and Zheltyhina, N.: Randolph Glacier Inventory – A Dataset of Global Glacier Outlines: Version 5.0: Technical Report, Colorado, USA., 2015.

Arino, O., Ramos Perez, J. J., Kalogirou, V., Bontemps, S., Defourny, P. and Van Bogaert, E.: Global Land Cover Map for 2009 (GlobCover 2009), , doi:https://doi.org/10.1594/PANGAEA.787668, 2012.

Armstrong, R. L., Rittger, K., Brodzik, M. J., Racoviteanu, A., Barrett, A. P., Khalsa, S.-J. S., Raup, B., Hill, A. F., Khan, A. L., Wilson, A. M., Kayastha, R. B., Fetterer, F. and Armstrong, B.: Runoff from glacier ice and seasonal snow in High Asia: separating melt water sources in river flow, Reg. Environ. Chang., 19, 1249–1261, doi:10.1007/s10113-018-1429-0, 2019.

Baba, M. W., Gascoin, S., Kinnard, C., Marchane, A. and Hanich, L.: Effect of digital elevation model resolution on the simulation of the snow cover evolution in the High Atlas, Water Resour. Res., 55, 1–19, doi:10.1029/2018WR023789, 2019.

Barnett, T. P., Adam, J. C. and Lettenmaier, D. P.: Potential impacts of a warming climate on water availability in snow-dominated regions, Nature, 438, 303–309, doi:10.1038/nature04141, 2005.

Bernhardt, M. and Schulz, K.: SnowSlide: A simple routine for calculating gravitational snow transport, Geophys. Res.

Lett., 37, L11502, doi:10.1029/2010GL043086, 2010.

Bernhardt, M., Schulz, K., Liston, G. E. and Zängl, G.: The influence of lateral snow redistribution processes on snow melt and sublimation in alpine regions, J. Hydrol., 424-425, 196–206, doi:10.1016/j.jhydrol.2012.01.001, 2012.

Best, M. J., Pryor, M., Clark, D. B., Rooney, G. G., Essery, R. L. H., Menard, C. B., Edwards, J. M., Hendry, M. A., Porson, A., Gedney, N., Mercado, L. M., Sitch, S., Blyth, E., Boucher, O., Cox, P. M., Grimmond, C. S. B. and Harding, R. J.: The Joint UK Land Environment Simulator (JULES), model description – Part 1 : Energy and water fluxes, Geosci. Model Dev., 4, 677–699, doi:10.5194/gmd-4-677-2011, 2011.

Biskop, S., Maussion, F., Krause, P. and Fink, M.: Differences in the water-balance components of four lakes in the southern-central Tibetan Plateau, Hydrol. Earth Syst. Sci., 20, 209–225, doi:10.5194/hess-20-209-2016, 2016.

Bonekamp, P. N. J., Collier, E. and Immerzeel, W. W.: The Impact of Spatial Resolution, Land Use, and Spinup Time on Resolving Spatial Precipitation Patterns in the Himalayas, J. Hydrometeorol., 19, 1565–1581, doi:10.1175/JHM-D-17-0212.1, 2018.

Bookhagen, B. and Burbank, D. W.: Toward a complete Himalayan hydrological budget: Spatiotemporal distribution of snowmelt and rainfall and their impact on river discharge, J. Geophys. Res., 115, F03019, doi:10.1029/2009JF001426, 2010.

Brown, M. E., Racoviteanu, A. E., Tarboton, D. G., Sen Gupta, A., Nigro, J., Policelli, F., Habib, S., Tokay, M., Shrestha, M. S., Bajracharya, S., Hummel, P., Gray, M., Duda, P., Zaitchik, B., Mahat, V., Artan, G. and Tokar, S.: An integrated modeling system for estimating glacier and snow melt driven streamflow from remote sensing and earth system data products in the Himalayas, J. Hydrol., 519, 1859–1869, doi:10.1016/j.jhydrol.2014.09.050, 2014.

Clark, M. P., Hendrikx, J., Slater, A. G., Kavetski, D., Anderson, B., Cullen, N. J., Kerr, T., Hreinsson, E. Ö. and Woods, R. A.: Representing spatial variability of snow water equivalent in hydrologic and land-surface models: A review, Water Resour. Res., 47, W07539, doi:10.1029/2011WR010745, 2011.

Clark, M. P., Nijssen, B., Lundquist, J. D., Kavetski, D., Rupp, D. E., Woods, R. A., Freer, J. E., Gutmann, E. D., Wood, A. W., Brekke, L. D., Arnold, J. R., Gochis, D. J. and Rasmussen, R. M.: A unified approach for process-based hydrologic modeling: 1. Modeling concept, Water Resour. Res., 51(4), 2498–2514, doi:10.1002/2015WR017200.A, 2015.

Collier, E. and Immerzeel, W. W.: High-resolution modeling of atmospheric dynamics in the Nepalese Himalaya, J. Geophys. Res. Atmos., 120, 9882–9896, doi:10.1002/2015JD023266, 2015.

Collier, E., Mölg, T., Maussion, F., Scherer, D., Mayer, C. and Bush, A. B. G.: High-resolution interactive modelling of the mountain glacier-atmosphere interface: an application over the Karakoram, Cryosph., 7, 779–795, doi:10.5194/tc-7-779-2013, 2013.

Collier, E., Maussion, F., Nicholson, L. I., Mölg, T., Immerzeel, W. W. and Bush, A. B. G.: Impact of debris cover on glacier ablation and atmosphere-glacier feedbacks in the Karakoram, Cryosph., 9, 1617–1632, doi:10.5194/tc-9-1617-2015, 2015.

Corripio, J. G.: Vectorial algebra algorithms for calculating terrain parameters from DEMs and solar radiation modelling in mountainous terrain, Int. J. Geogr. Inf. Sci., 17(1), 1–23, doi:10.1080/713811744, 2003.

Cox, P. M., Betts, R. A., Bunton, C. B., Essery, R. L. H., Rowntree, P. R. and Smith, J.: The impact of new land surface physics on the GCM simulation of climate and climate sensitivity, Clim. Dyn., 15(3), 183–203, doi:10.1007/s003820050276, 1999.

Douville, H., Royer, J.-F. and Mahfouf, J.-F.: A new snow parameterization for the Météo-France climate model. Part I: validation in stand-alone experiments, Clim. Dyn., 12(1), 21–35, doi:10.1007/BF00208760, 1995.

Duethmann, D., Zimmer, J., Gafurov, A., Güntner, A., Kriegel, D., Merz, B. and Vorogushyn, S.: Evaluation of areal precipitation estimates based on downscaled reanalysis and station data by hydrological modelling, Hydrol. Earth Syst. Sci., 17, 2415–2434, doi:10.5194/hess-17-2415-2013, 2013.

Dutra, E., Balsamo, G., Viterbo, P., Miranda, P. M., Beljaars, A., Schär, C. and Elder, K.: An improved snow scheme for the ECMWF land surface model: Description and offline validation, J. Hydrometeorol., 11(4), 899–916, doi:10.1175/2010JHM1249.1, 2010.

Essery, R.: Large-scale simulations of snow albedo masking by forests, Geophys. Res. Lett., 40, 5521–5525, doi:10.1002/grl.51008, 2013.

Essery, R.: A factorial snowpack model (FSM 1.0), Geosci. Model Dev., 8, 3867–3876, doi:10.5194/gmd-8-3867-2015, 2015.

Essery, R., Rutter, N., Pomeroy, J., Baxter, R., Stähli, M., Gustafsson, D., Barr, A., Bartlett, P. and Elder, K.: SNOWMIP2: An Evaluation of Forest Snow Process Simulations, Bull. Am. Meteorol. Soc., 90(8), 1120–1135, doi:https://doi.org/10.1175/2009BAMS2629.1, 2009.

Essery, R., Morin, S., Lejeune, Y. and Ménard, C. B.: A comparison of 1701 snow models using observations from an alpine site, Adv. Water Resour., 55, 131–148, doi:10.1016/j.advwatres.2012.07.013, 2013.

Etchevers, P., Martin, E., Brown, R., Fierz, C., Lejeune, Y., Bazile, E., Boone, A., Dai, Y., Essery, R., Fernandez, A., Gusev, Y., Jordan, R., Koren, V., Kowalczyk, E., Nasonova, N. O., Pyles, R. D., Schlosser, A., Shmakin, A. B., Smirnova, T. G., Strasser, U., Verseghy, D., Yamazaki, T. and Yang, Z.-L.: Validation of the energy budget of an alpine snowpack simulated by several snow models (SnowMIP project), Ann. Glaciol., 38, 150–158, doi:https://doi.org/10.3189/172756404781814825, 2004.

Finger, D., Pellicciotti, F., Konz, M., Rimkus, S. and Burlando, P.: The value of glacier mass balance, satellite snow cover images, and hourly discharge for improving the performance of a physically based distributed hydrological model, Water Resour. Res., 47, W07519, doi:10.1029/2010WR009824, 2011.

Fowler, H. J. and Archer, D. R.: Hydro-climatological variability in the Upper Indus Basin and implications for water resources, in Regional Hydrological Impacts of Climatic Change - Impact Assessment and Decision Making (Proceedings of symposium S6 held during the Seventh IAHS Scientific Assembly at Foz do Iguacu, Brazil, April 2005), IAHS Publ. 295, Foz do Iguacu, Brazil., 2005.

Gafurov, A. and Bárdossy, A.: Cloud removal methodology from MODIS snow cover product, Hydrol. Earth Syst. Sci., 13, 1361–1373, doi:10.5194/hess-13-1361-2009, 2009.

https://doi.org/10.5194/tc-2019-187
Preprint. Discussion started: 10 September 2019

Gascoin, S., Guðmundsson, S., Aðalgeirsdóttir, G., Pálsson, F., Schmidt, L., Berthier, E. and Björnsson, H.: Evaluation of MODIS Albedo Product over Ice Caps in Iceland and Impact of Volcanic Eruptions on Their Albedo, Remote Sens., 9(399), 1–18, doi:10.3390/rs9050399, 2017.

Günther, D., Marke, T., Essery, R. and Strasser, U.: Uncertainties in Snowpack Simulations—Assessing the Impact of Model Structure, Parameter Choice, and Forcing Data Error on Point-Scale Energy Balance Snow Model Performance, Water Resour. Res., 55, 2779–2800, doi:10.1029/2018WR023403, 2019.

Hall, A. and Qu, X.: Using the current seasonal cycle to constrain snow albedo feedback in future climate change, Geophys. Res. Lett., 33, L03502, doi:10.1029/2005GL025127, 2006.

Hall, D. K. and Riggs, G. A.: MODIS/Terra Snow Cover Daily L3 Global 500m Grid, Version 6. [2000-2015], , doi:10.5067/MODIS/MOD10A1.006, 2016.

Harder, P., Pomeroy, J. W. and Helgason, W.: Local-Scale Advection of Sensible and Latent Heat During Snowmelt, Geophys. Res. Lett., 44, 9769–9777, doi:10.1002/2017GL074394, 2017.

Havens, S., Marks, D., FitzGerald, K., Masarik, M., Flores, A. N., Kormos, P. and Hedrick, A.: Approximating Input Data to a Snowmelt Model Using Weather Research and Forecasting Model Outputs in Lieu of Meteorological Measurements, J. Hydrometeorol., 20(5), 847–862, doi:10.1175/JHM-D-18-0146.1, 2019.

Hewitt, K.: Glaciers of the Karakoram Himalaya, Springer Netherlands., 2014.

Huintjes, E., Sauter, T., Schröter, B., Maussion, F., Yang, W., Kropáček, J., Buchroithner, M., Scherer, D., Kang, S. and Schneider, C.: Evaluation of a coupled snow and energy balance model for Zhadang glacier, Tibetan Plateau, using glaciological measurements and time-lapse photography, Arctic, Antarct. Alp. Res., 47(3), 573–590, doi:10.1657/AAAR0014-073, 2015.

Immerzeel, W. W., van Beek, L. P. H. and Bierkens, M. F. P.: Climate Change Will Affect the Asian Water Towers, Science (80-.)., 382, 1382–1385, doi:10.1126/science.1183188, 2010.

Jarvis, A., Reuter, H. I., Nelson, A. and Guevara, E.: Hole-filled SRTM for the globe Version 4, available from the CGIAR-CSI SRTM 90m Database (http://srtm.csi.cgiar.org), 2008.

Klemeš, V.: The modelling of mountain hydrology: the ultimate challenge, Hydrol. Mt. Areas (Proceedings Štrbské Pleso Work. Czechoslov. June 1989), IAHS 190, 29–44, 1990.

Krinner, G., Derksen, C., Essery, R., Flanner, M., Hagemann, S., Clark, M., Hall, A., Rott, H., Brutel-Vuilmet, C., Kim, H., Ménard, C. B., Mudryk, L., Thackeray, C., Wang, L., Arduini, G., Balsamo, G., Bartlett, P., Boike, J., Boone, A., Chéruy, F., Colin, J., Cuntz, M., Dai, Y., Decharme, B., Derry, J., Ducharne, A., Dutra, E., Fang, X., Fierz, C., Ghattas, J., Gusev, Y., Haverd, V., Kontu, A., Lafaysse, M., Law, R., Lawrence, D., Li, W., Marke, T., Marks, D., Ménégoz, M., Nasonova, O., Nitta, T., Niwano, M., Pomeroy, J., Raleigh, M. S., Schaedler, G., Semenov, V., Smirnova, T. G., Stacke, T., Strasser, U., Svenson, S., Turkov, D., Wang, T., Wever, N., Yuan, H., Zhou, W. and Zhu, D.: ESM-SnowMIP: assessing snow models and quantifying snow-related climate feedbacks, Geosci. Model Dev., 11, 5027–5049, doi:10.5194/gmd-11-5027-2018, 2018.

https://doi.org/10.5194/tc-2019-187
Preprint. Discussion started: 10 September 2019

Lafaysse, M., Cluzet, B., Dumont, M., Lejeune, Y., Vionnet, V. and Morin, S.: A multiphysical ensemble system of numerical snow modelling, Cryosph., 11, 1173–1198, doi:10.5194/tc-11-1173-2017, 2017.

Lapo, K., Nijssen, B. and Lundquist, J. D.: Evaluation of Turbulence Stability Schemes of Land Models for Stable Conditions, J. Geophys. Res. Atmos., 124, 3072–3089, doi:10.1029/2018JD028970, 2019.

Lehning, M., Ingo, V., Gustafsson, D., Nguyen, T. A., Stähli, M. and Zappa, M.: ALPINE3D: a detailed model of mountain surface processes and its application to snow hydrology, Hydrol. Process., 20, 2111–2128, doi:10.1002/hyp.6204, 2006.

Liston, G. E. and Elder, K.: A Distributed Snow-Evolution Modeling System (SnowModel), J. Hydrometeorol., 7, 1259–1276, doi:10.1175/JHM548.1, 2006a.

Liston, G. E. and Elder, K.: A Meteorological Distribution System for High-Resolution Terrestrial Modeling (MicroMet), J. Hydrometeorol., 7, 217–234, doi:10.1175/JHM486.1, 2006b.

Litt, M., Shea, J., Wagnon, P., Steiner, J., Koch, I., Stigter, E. and Immerzeel, W.: Glacier ablation and temperature indexed melt models in the Nepalese Himalaya, Sci. Rep., 9, 5264, doi:10.1038/s41598-019-41657-5, 2019.

Liu, J., Schaaf, C., Strahler, A., Jiao, Z., Shuai, Y., Zhang, Q., Roman, M., Augustine, J. A. and Dutton, E. G.: Validation of Moderate Resolution Imaging Spectroradiometer (MODIS) albedo retrieval algorithm: Dependence of albedo on solar zenith angle, J. Geophys. Res., 114, D01106, doi:10.1029/2008JD009969, 2009.

Lundquist, J. D., Dettinger, M. D. and Cayan, D. R.: Snow-fed streamflow timing at different basin scales: Case study of the Tuolumne River above Hetch Hetchy, Yosemite, California, Water Resour. Res., 41, W07005, doi:10.1029/2004WR003933, 2005.

Lute, A. C. and Luce, C. H.: Are Model Transferability and Complexity Antithetical? Insights from Validation of a Variable-Complexity Empirical Snow Model in Space and Time, Water Resour. Res., 53(11), 8825–8850, doi:10.1002/2017WR020752, 2017.

Lutz, A. F., Immerzeel, W. W., Shrestha, A. B. and Bierkens, M. F. P.: Consistent increase in High Asia's runoff due to increasing glacier melt and precipitation, Nat. Clim. Chang., 4, 587–592, doi:10.1038/NCLIMATE2237, 2014.

Lutz, A. F., Immerzeel, W. W., Kraaijenbrink, P. D. A., Shrestha, A. B. and Bierkens, M. F. P.: Climate Change Impacts on the Upper Indus Hydrology: Sources, Shifts and Extremes, PLoS One, 11(11), 1–33, doi:10.1371/journal.pone.0165630, 2016.

Magnusson, J., Wever, N., Essery, R., Helbig, N., Winstral, A. and Jonas, T.: Evaluating snow models with varying process representations for hydrological applications, Water Resour. Res., 51, 2707–2723, doi:10.1002/2014WR016498, 2015.

Maussion, F., Scherer, D., Mölg, T., Collier, E., Curio, J. and Finkelnburg, R.: Precipitation Seasonality and Variability over the Tibetan Plateau as Resolved by the High Asia Reanalysis, J. Clim., 27, 1910–1927, doi:10.1175/JCLI-D-13-00282.1, 2014.

Moeser, D., Mazzotti, G., Helbig, N. and Jonas, T.: Representing spatial variability of forest snow: Implementation of a

new interception model, Water Resour. Res., 52, 1208–1226, doi:10.1002/2015WR017961, 2016.

Mukhopadhyay, B. and Khan, A.: Altitudinal variations of temperature, equilibrium line altitude, and accumulation-area ratio in Upper Indus Basin, Hydrol. Res., 48(1), 214–230, doi:10.2166/nh.2016.144, 2016.

Musselman, K. N., Pomeroy, J. W., Essery, R. L. H. and Leroux, N.: Impact of windflow calculations on simulations of alpine snow accumulation, redistribution and ablation, Hydrol. Process., 29, 3983–3999, doi:10.1002/hyp.10595, 2015.

Musselman, K. N., Clark, M. P., Liu, C., Ikeda, K. and Rasmussen, R.: Slower snowmelt in a warmer world, Nat. Clim. Chang., 7, 214–220, doi:10.1038/NCLIMATE3225, 2017.

Naden, P. S.: Spatial variability in flood estimation for large catchments: the exploitation of channel network structure, Hydrol. Sci. J., 37(1), 53–72, doi:10.1080/02626669209492561, 1992.

Niu, G. Y., Yang, Z. L., Mitchell, K. E., Chen, F., Ek, M. B., Barlage, M., Kumar, A., Manning, K., Niyogi, D., Rosero, E., Tewari, M. and Xia, Y.: The community Noah land surface model with multiparameterization options (Noah-MP): 1 . Model description and evaluation with local-scale measurements, J. Geophys. Res., 116, D12109, doi:10.1029/2010JD015139, 2011.

Oleson, K. W., Lawrence, D. M., Bonan, G. B., Drewniak, B., Huang, M., Koven, C. D., Levis, S., Li, F., Riley, W. J., Subin, Z. M., Swenson, S. C., Thornton, P. E., Bozbiyik, A., Fisher, R., Kluzek, E., Lamarque, J.-F., Lawrence, P. J., Leung, L. R., Lipscomb, W., Muszala, S., Ricciuto, D. M., Sacks, W., Sun, Y., Tang, J. and Yang, Z.-L.: Technical Description of version 4.5 of the Community Land Model (CLM). NCAR Technical Note NCAR/TN-503+STR, Boulder, Colorado, USA., 2013.

Palazzi, E., Filippi, L. and Hardenberg, J. Von: Insights into elevation-dependent warming in the Tibetan Plateau-Himalayas from CMIP5 model simulations, Clim. Dyn., 48(11), 3991–4008, doi:10.1007/s00382-016-3316-z, 2017.

Pepin, N., Bradley, R., Diaz, H. F., Baraer, M., Caceres, E. B., Forsythe, N., Fowler, H. J., Greenwood, G., Hashmi, M. Z., Liu, X. D., Miller, J. R., Ning, L., Ohmura, A., Palazzi, E., Rangwala, I., Schoener, W., Severskiy, I., Shahgedanova, M., Wang, M. B., Williamson, S. N. and Yang, D. Q.: Elevation-dependent warming in mountain regions of the world, Nat. Clim. Chang., 5, 424–430, doi:10.1038/nclimate2563, 2015.

Prasch, M., Mauser, W. and Weber, M.: Quantifying present and future glacier melt-water contribution to runoff in a central Himalayan river basin, Cryosph., 7, 889–904, doi:10.5194/tc-7-889-2013, 2013.

Pritchard, D. M. W., Forsythe, N., Fowler, H. J., O'Donnell, G. M. and Li, X.-F.: Evaluation of Upper Indus Near-Surface Climate Representation by WRF in the High Asia Refined Analysis, J. Hydrometeorol., 20(3), 467–487, doi:10.1175/JHM-D-18-0030.1, 2019.

Quéno, L., Vionnet, V., Dombrowski-Etchevers, I., Lafaysse, M., Dumont, M. and Karbou, F.: Snowpack modelling in the Pyrenees driven by kilometric- resolution meteorological forecasts, Cryosph., 10, 1571–1589, doi:10.5194/tc-10-1571-2016, 2016.

Ragettli, S., Pellicciotti, F., Bordoy, R. and Immerzeel, W. W.: Sources of uncertainty in modeling the glaciohydrological response of a Karakoram watershed to climate change, Water Resour. Res., 49, 6048–6066,

doi:10.1002/wrcr.20450, 2013.

Ragettli, S., Pellicciotti, F., Immerzeel, W. W., Miles, E. S., Petersen, L., Heynen, M., Shea, J. M., Stumm, D., Joshi, S. and Shrestha, A.: Unraveling the hydrology of a Himalayan catchment through integration of high resolution in situ data and remote sensing with an advanced simulation model, Adv. Water Resour., 78, 94–111, doi:10.1016/j.advwatres.2015.01.013, 2015.

Raleigh, M. S., Lundquist, J. D. and Clark, M. P.: Exploring the impact of forcing error characteristics on physically based snow simulations within a global sensitivity analysis framework, Hydrol. Earth Syst. Sci., 19, 3153–3179, doi:10.5194/hess-19-3153-2015, 2015.

Raleigh, M. S., Livneh, B., Lapo, K. and Lundquist, J. D.: How Does Availability of Meteorological Forcing Data Impact Physically Based Snowpack Simulations?, J. Hydrometeorol., 17, 99–120, doi:10.1175/JHM-D-14-0235.1, 2016.

Revuelto, J., Lafaysse, M., Zin, I., Charrois, L., Vionnet, V., Dumont, M., Rabatel, A., Six, D., Condom, T., Morin, S., Viani, A. and Sirguey, P.: Multi-Criteria Evaluation of Snowpack Simulations in Complex Alpine Terrain Using Satellite and In Situ Observations, Remote Sens., 10(1171), 1–32, doi:10.3390/rs10081171, 2018.

Rutter, N., Essery, R., Pomeroy, J., Altimir, N., Andreadis, K., Baker, I., Barr, A., Bartlett, P., Boone, A., Deng, H., Douville, H., Dutra, E., Elder, K., Ellis, C., Feng, X., Gelfan, A., Goodbody, A., Gusev, Y., Gustafsson, D., Hellström, R., Hirabayashi, Y., Hirota, T., Jonas, T., Koren, V., Kuragina, A., Lettenmaier, D., Li, W., Luce, C., Martin, E., Nasonova, O., Pumpanen, J., Pyles, R. D., Samuelsson, P., Sandells, M., Schädler, G., Shmakin, A., Smirnova, T. G., Stähli, M., Stöckli, R., Strasser, U., Su, H., Suzuki, K., Takata, K., Tanaka, K., Thompson, E., Vesala, T., Viterbo, P., Wiltshire, A., Xia, K., Xue, Y. and Yamazaki, T.: Evaluation of forest snow processes models (SnowMIP2), J. Geophys. Res., 114, D06111, doi:10.1029/2008JD011063, 2009.

Salomonson, V. V and Appel, I.: Estimating fractional snow cover from MODIS using the normalized difference snow index, Remote Sens. Environ., 89, 351–360, doi:10.1016/j.rse.2003.10.016, 2004.

Shakoor, A. and Ejaz, N.: Flow Analysis at the Snow Covered High Altitude Catchment via Distributed Energy Balance Modeling, Sci. Rep., 9(4783), 1–14, doi:10.1038/s41598-019-39446-1, 2019.

Sharif, M., Archer, D. R., Fowler, H. J. and Forsythe, N.: Trends in timing and magnitude of flow in the Upper Indus Basin, Hydrol. Earth Syst. Sci., 17, 1503–1516, doi:10.5194/hess-17-1503-2013, 2013.

Shrestha, M., Koike, T., Hirabayashi, Y., Xue, Y., Wang, L., Rasul, G. and Ahmad, B.: Integrated simulation of snow and glacier melt in water and energy balance-based, distributed hydrological modeling framework at Hunza River Basin of Pakistan Karakoram region, J. Geophys. Res. Atmos., 120(10), 4889–4919, doi:10.1002/2014JD022666, 2015.

Sicart, J. E., Pomeroy, J. W., Essery, R. L. H. and Bewley, D.: Incoming longwave radiation to melting snow: observations, sensitivity and estimation in northern environments, Hydrol. Process., 20, 3697–3708, doi:10.1002/hyp.6383, 2006.

Skamarock, W. C., Klemp, J. B., Dudhia, J., Gill, D. O., Barker, D. M., Duda, M. G., Huang, X.-Y., Wang, W. and Power, J. G.: A Description of the Advanced Research WRF Version 3, NCAR Technical Note NCAR/TN–475+STR., 2008.

https://doi.org/10.5194/tc-2019-187
Preprint. Discussion started: 10 September 2019

Slater, A. G., Schlosser, C. A., Desborough, C. E., Pitman, A. J., Henderson-Sellers, A., Robock, A., Vinnikov, K. Y., Mitchell, K., Boone, A., Braden, H., Chen, F., Cox, P. M., de Rosnay, P., Dickinson, R. E., Dai, Y.-J., Duan, Q., Entin, J., Etchevers, P., Gedney, N., Gusev, Y. M., Kim, J., Koren, V., Kowalczyk, E. A., Nasonova, O. N., Noilhan, J., Schaake, S., Shmakin, A. B., Smirnova, T. G., Verseghy, D., Wetzel, P., Xue, Y., Yang, Z.-L. and Zeng, Q.: The Representation of Snow in Land Surface Schemes: Results from PILPS 2 (d), J. Hydrometeorol., 2, 7–25, doi:10.1175/1525-7541(2001)002<0007:TROSIL>2.0.CO;2, 2001.

Sohrabi, M. M., Tonina, D., Benjankar, R., Kumar, M., Kormos, P., Marks, D. and Luce, C.: On the role of spatial resolution on snow estimates using a process-based snow model across a range of climatology and elevation, Hydrol. Process., 33, 1260–1275, doi:10.1002/hyp.13397, 2019.

Stigter, E. E., Wanders, N., Saloranta, T. M., Shea, J. M., Bierkens, M. F. P. and Immerzeel, W. W.: Assimilation of snow cover and snow depth into a snow model to estimate snow water equivalent and snowmelt runoff in a Himalayan catchment, Cryosph., 11, 1647–1664, doi:10.5194/tc-11-1647-2017, 2017.

Stigter, E. E., Litt, M., Steiner, J. F., Bonekamp, P. N. J., Shea, J. M., Bierkens, M. F. P. and Immerzeel, W. W.: The Importance of Snow Sublimation on a Himalayan Glacier, Front. Earth Sci., 6, 108, doi:10.3389/feart.2018.00108, 2018.

Strasser, U., Bernhardt, M., Weber, M., Liston, G. E. and Mauser, W.: Is snow sublimation important in the alpine water balance?, Cryosph., 2, 53–66, doi:10.5194/tc-2-53-2008, 2008.

Tarasova, L., Knoche, M., Dietrich, J. and Merz, R.: Effects of input discretization, model complexity, and calibration strategy on model performance in a data-scarce glacierized catchment in Central Asia, Water Resour. Res., 52, 4674–4699, doi:10.1002/2015WR018551, 2016.

Verseghy, D. L.: CLASS—A Canadian land surface scheme for GCMs. I. Soil model, Int. J. Climatol., 11(2), 111–133, doi:10.1002/joc.3370110202, 1991.

Vionnet, V., Brun, E., Morin, S., Boone, A., Faroux, S., Le Moigne, P., Martin, E. and Willemet, J.-M.: The detailed snowpack scheme Crocus and its implementation in SURFEX v7.2, Geosci. Model Dev., 5, 773–791, doi:10.5194/gmd-5-773-2012, 2012.

Vionnet, V., Martin, E., Masson, V., Guyomarc'h, G., Naaim-Bouvet, F., Prokop, A., Durand, Y. and Lac, C.: Simulation of wind-induced snow transport and sublimation in alpine terrain using a fully coupled snowpack/atmosphere model, Cryosph., 8, 395–415, doi:10.5194/tc-8-395-2014, 2014.

Viviroli, D., Archer, D. R., Buytaert, W., Fowler, H. J., Greenwood, G. B., Hamlet, A. F., Huang, Y., Koboltschnig, G., Litaor, M. I., López-Moreno, J. I., Lorentz, S., Schädler, B., Schreier, H., Schwaiger, K., Vuille, M. and Woods, R.: Climate change and mountain water resources: overview and recommendations for research, management and policy, Hydrol. Earth Syst. Sci., 15, 471–504, doi:10.5194/hess-15-471-2011, 2011.

Wan, Z.: New refinements and validation of the collection-6 MODIS land-surface temperature/emissivity product, Remote Sens. Environ., 140, 36–45, doi:10.1016/j.rse.2013.08.027, 2014.

Wan, Z., Zhang, Y., Zhang, Q. and Li, Z.-L.: Quality assessment and validation of the MODIS global land surface

https://doi.org/10.5194/tc-2019-187
Preprint. Discussion started: 10 September 2019

temperature, Int. J. Remote Sens., 25(1), 261–274, doi:10.1080/0143116031000116417, 2004.

Wang, Z., Schaaf, C. B., Chopping, M. J., Strahler, A. H., Wang, J., Román, M. O., Rocha, A. V, Woodcock, C. E. and Shuai, Y.: Evaluation of Moderate-resolution Imaging Spectroradiometer (MODIS) snow albedo product (MCD43A) over tundra, Remote Sens. Environ., 117, 264–280, doi:10.1016/j.rse.2011.10.002, 2012.

Waqas, A. and Athar, H.: Observed diurnal temperature range variations and its association with observed cloud cover in northern Pakistan, Int. J. Climatol., 38(8), 3323–3336, doi:10.1002/joc.5503, 2018.

Wen, J., Liu, Q., Xiao, Q., Liu, Q., You, D., Hao, D., Wu, S. and Lin, X.: Characterizing Land Surface Anisotropic Reflectance over Rugged Terrain: A Review of Concepts and Recent Developments, Remote Sens., 10(370), 1–30, doi:10.3390/rs10030370, 2018.

Winstral, A., Marks, D. and Gurney, R.: Assessing the Sensitivities of a Distributed Snow Model to Forcing Data Resolution, J. Hydrometeorol., 15(4), 1366–1383, doi:10.1175/JHM-D-13-0169.1, 2014.

https://doi.org/10.5194/tc-2019-187
Preprint. Discussion started: 10 September 2019


The Cryosphere Discussions
Open Access
EGU

Process Description	Short Name	Parameterisation 0	Parameterisation 1
Snow albedo variation	Albedo (AL)	Diagnostic – function of surface temperature	Prognostic – decays with time and increases with snowfall
Density of fresh snow and snowpack density evolution	Density (DE)	Constant	Specified fresh snow density and compaction increases with time
Liquid water storage, drainage and refreezing	Liquid Water (LW)	Instant drainage, no refreezing	Bucket model (drainage to layer below if liquid holding capacity exceeded), with refreezing (and latent heat release) accounted for
Atmospheric stability adjustment for turbulent heat fluxes	Stability (ST)	No adjustment for atmospheric stability	Stability factor is a function of the bulk Richardson number, which quantifies the extent to which buoyancy suppresses shear production of turbulent fluxes
Thermal conductivity for heat conduction	Thermal Conductivity (TC)	Constant	Function of density

Table 1. Summary of the process parameterisation options available in FSM. Full details are provided in Essery (2015). The short names and abbreviations by which the processes are referred to in the text and figures are given.

https://doi.org/10.5194/tc-2019-187
Preprint. Discussion started: 10 September 2019

The Cryosphere Discussions
Open Access
EGU

Variable	Month / Process											
	April			May			June			July		
	AL	LW	ST	AL	LW	ST	AL	LW	ST	AL	LW	ST
Albedo (-)	0.12	0.00	0.00	0.15	0.00	0.00	0.12	0.00	0.00	0.07	0.00	0.00
Melt (mm/d)	-3.5	1.0	0.2	-5.2	1.9	-0.3	-4.3	2.7	-4.6	-0.1	3.5	-7.7
Snowpack Runoff (mm/d)	-2.2	-1.9	0.0	-2.7	-1.6	-0.2	0.0	0.6	-1.0	2.8	1.4	0.1
SCA (-)	0.04	0.02	0.02	0.08	0.04	0.04	0.12	0.06	0.07	0.10	0.05	0.09
Snowpack Temperature (°C)	-0.6	3.5	-1.9	-0.4	6.3	-1.6	0.1	7.3	-1.5	0.3	8.1	-1.1
Surface Temperature (°C)	0.1	0.9	-2.9	0.3	1.4	-3.2	0.4	1.5	-3.9	0.5	1.3	-3.6
Sensible Heat Flux (W m^{-2})	0.6	-1.2	-22.0	0.8	-1.6	-25.9	1.5	-0.7	-46.6	3.1	0.4	-49.4
Net Turbulent Fluxes (W m^{-2})	1.2	-2.4	-16.0	1.3	-3.0	-18.9	2.0	-1.8	-36.8	4.4	-0.3	-52.7
Net Radiation (W m-2)	-13.0	-1.8	12.3	-20.1	-2.9	13.8	-18.1	-2.0	16.2	-3.7	0.3	20.0

Table 2. Catchment-scale mean differences (option 1 – option 0) for key states and fluxes in selected months. Differences are calculated separately for the albedo (AL), liquid water (LW) and stability adjustment (ST) parameterisations. Albedo differences are at solar noon and average snowpack temperatures are weighted by snow depth.

5

https://doi.org/10.5194/tc-2019-187
Preprint. Discussion started: 10 September 2019

Error ID	SCA Errors	Explanation
i	Underestimation of the negative spring/summer SCA anomaly in 2001.	The contemporaneous and preceding (negative) precipitation anomalies are reasonable, but the HAR does not capture the strongly positive temperature anomalies. Under these erroneously cool simulated conditions, the faster-responding configurations result in lower errors than the more physically realistic, slower-responding configurations (i.e. prognostic albedo and a representation of liquid water processes).
ii	Positive simulated SCA anomaly in summer 2002 exceeds the neutral anomaly suggested by MODIS.	The HAR inputs provide a positive spring precipitation anomaly that far exceeds the observed anomaly, while again offering too negative a temperature anomaly. These conditions are conducive to slow melt of the excessive spring snowfall, which helps to explain the poorer performance of the slower-responding configurations.
iii	Positive simulated SCA anomaly in late-summer/autumn 2005 contrasts with a negative anomaly from MODIS.	This is likely due at least partly to HAR overestimation of precipitation in the preceding winter and spring, as well as potentially in the concurrent summer. The HAR may also underestimate the temperature anomaly in the crucial summer months.
iv	Positive late-summer/autumn SCA anomaly in 2008 in MODIS is not reproduced by the model.	The magnitude of the positive precipitation anomaly at this time seems to be underestimated by the HAR, which also provides too positive a temperature anomaly. This would be conducive to melt of early snowfall and underestimation of the positive SCA anomaly. Unlike the summer examples, the resulting absolute errors are similar for all configurations, which reflects persistent challenges in simulating the timing of early autumn/winter snowfall.
vi	The magnitude of the strong positive summer SCA anomaly in 2010 is underestimated.	This coincides with the largest spread in simulated anomalies in the series. Precipitation anomalies in the preceding winter and spring are underestimated, along with the large summer anomaly, which coincided with devastating floods in Pakistan). Summer temperature anomalies are notably overestimated. All configurations underestimate summer SCA by varying degrees.

Table 3. Assessment of SCA time series errors in Figure 8 and their relationships with climate anomalies. Error IDs correspond with Figure 8.

https://doi.org/10.5194/tc-2019-187
Preprint. Discussion started: 10 September 2019

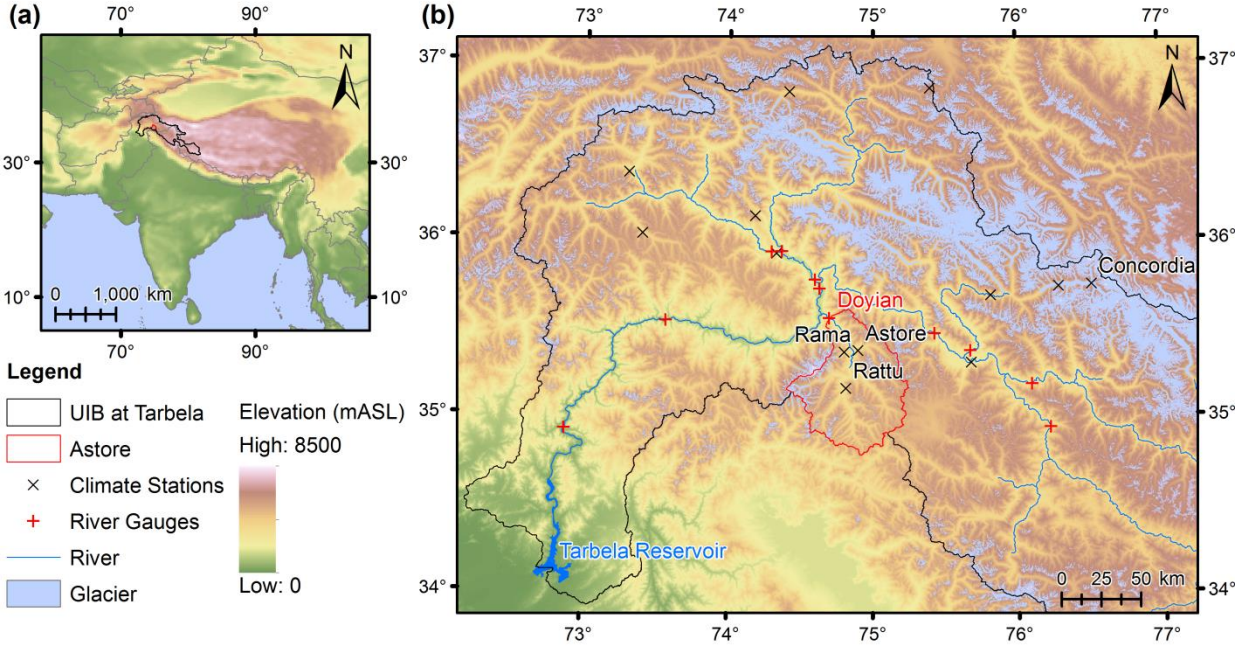

Figure 1. Location of study area and local measurement points. The regional context is indicated in (a). The Astore catchment and observation locations (with labels for the most important sites in this study) are shown with topography and glacier extent in (b).

https://doi.org/10.5194/tc-2019-187
Preprint. Discussion started: 10 September 2019

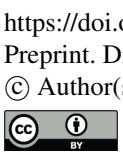

The Cryosphere Discussions
Open Access
EGU

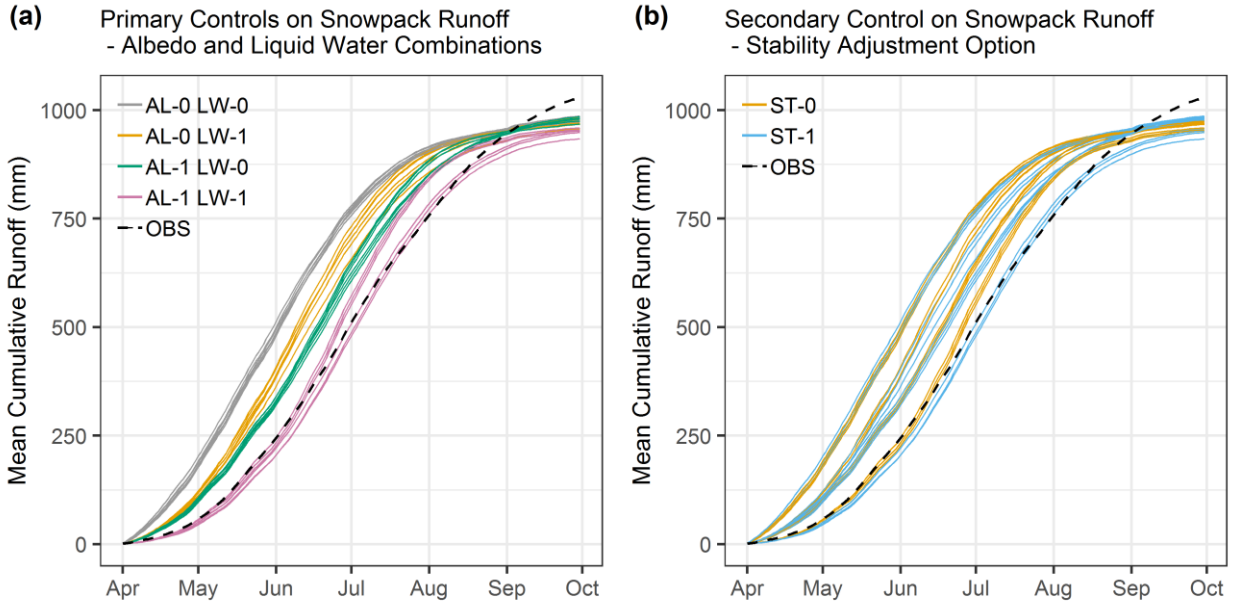

Figure 2. Comparison of mean cumulative snowpack runoff for the high-flow season for each of the 32 ensemble members with observed total runoff (OBS, black dashed line). In (a) each ensemble member is coloured according to the combination of albedo (AL) and liquid water (LW) parameterisations it uses. In (b) each ensemble member is coloured by its stability adjustment (ST) option.

5

https://doi.org/10.5194/tc-2019-187
Preprint. Discussion started: 10 September 2019

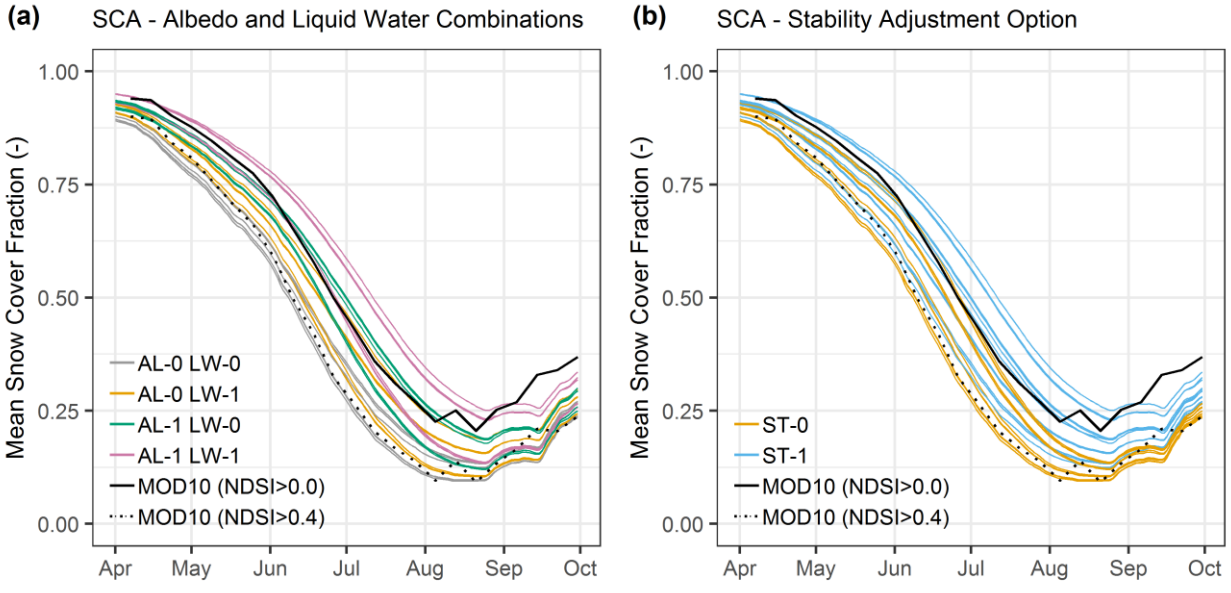

Figure 3. Similar to Figure 2 but for catchment snow-covered area (SCA). The two MODIS MOD10A1 series shown are based on Normalised Difference Snow Index (NDSI) thresholds of 0.0 (solid line) and 0.4 (dotted line).

https://doi.org/10.5194/tc-2019-187
Preprint. Discussion started: 10 September 2019

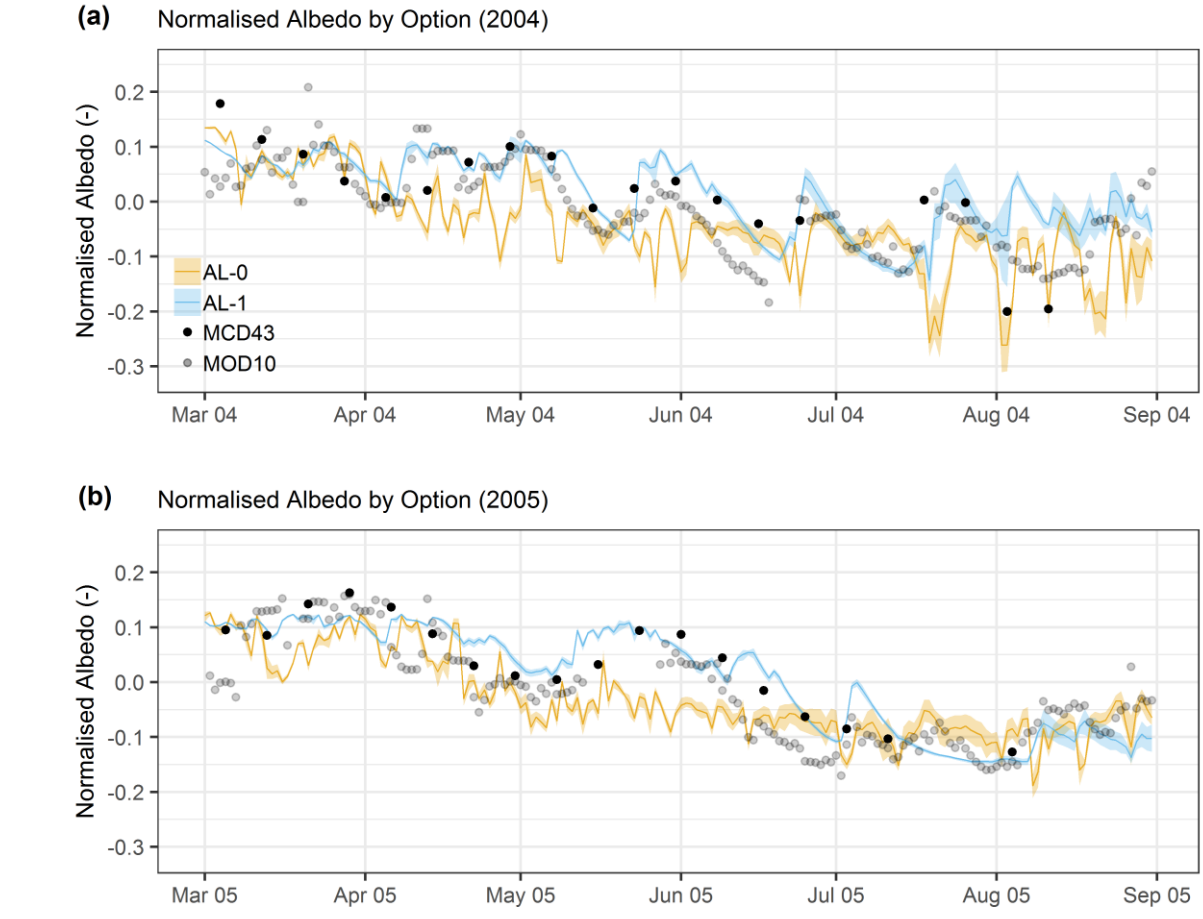

Figure 4. Comparison of modelled catchment-average snow albedo with MODIS remote sensing for two example melt seasons. Modelled albedo is grouped by the diagnostic (0) and prognostic (1) options in orange and blue, respectively. The mean (line) and range (shading) for the two groups are shown. MCD43A3 and MOD10A1 (8-day moving average) estimates are denoted with black and grey dots, respectively. The modelled series are normalised by subtracting the ensemble mean albedo (all members), while the MODIS series are normalised by subtracting their respective means.

https://doi.org/10.5194/tc-2019-187
Preprint. Discussion started: 10 September 2019

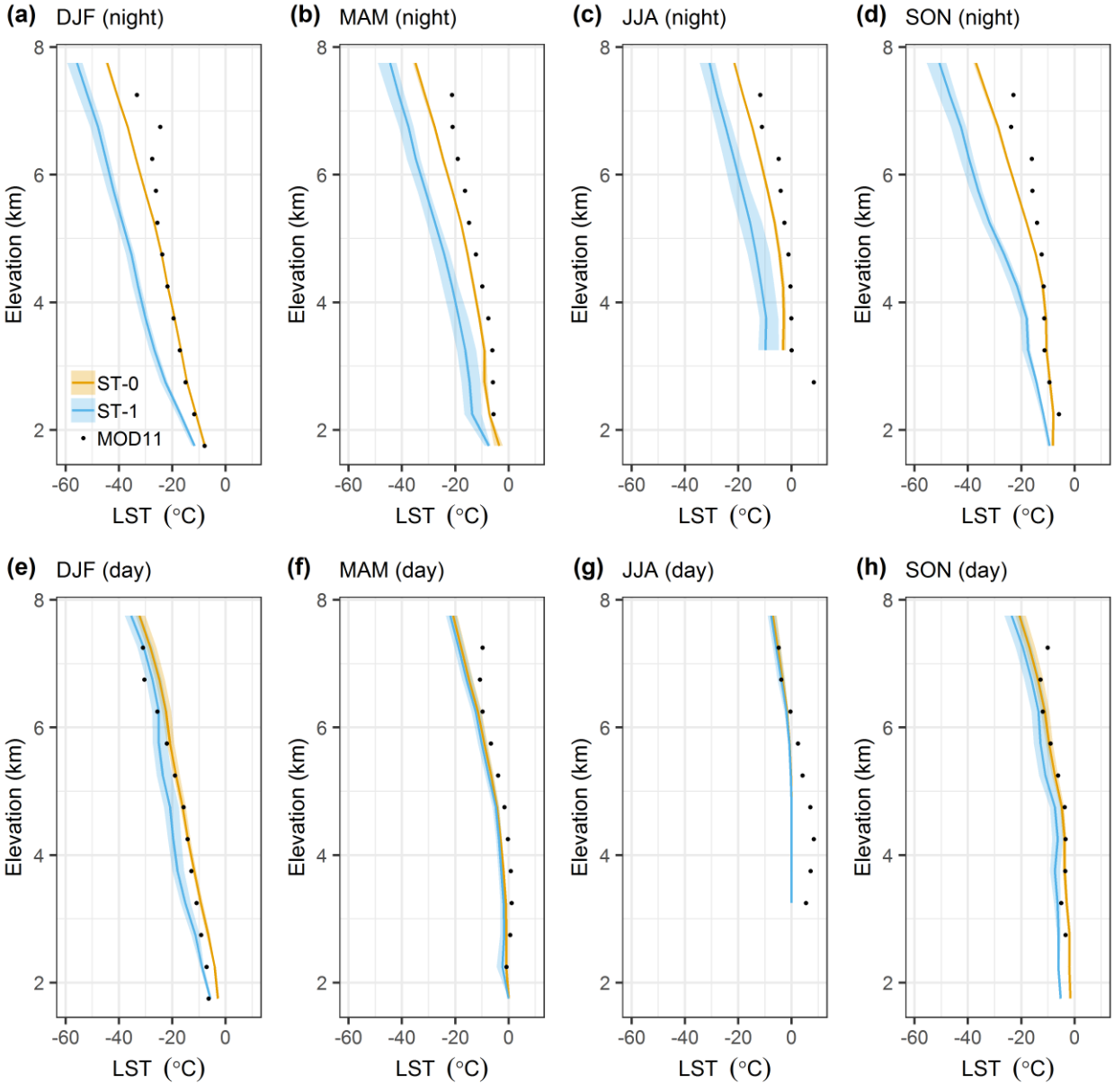

Figure 5. Comparison of modelled seasonal mean elevation profiles of LST with MODIS MOD11A1 remote sensing. The ensemble members are grouped by stability adjustment option (mean and range of groups shown). The top and bottom rows show night-time and day-time temperatures, respectively. Model results correspond with the closest model time step to the Terra platform overpass times, as well as only days for which MODIS retrievals are available (i.e. clear-sky conditions).

https://doi.org/10.5194/tc-2019-187
Preprint. Discussion started: 10 September 2019

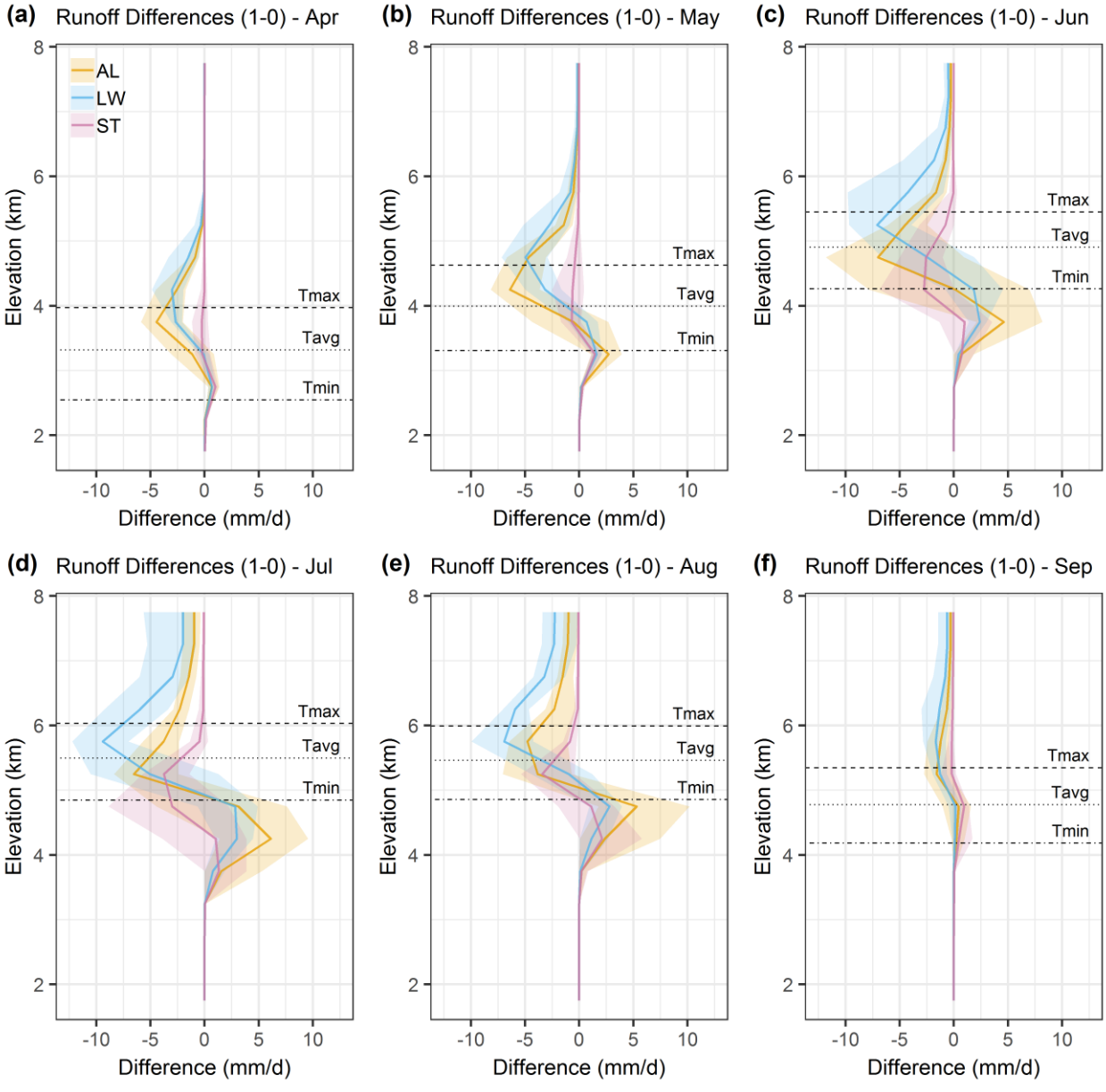

Figure 6. Spatial (vertical) and temporal (monthly) differences in simulated runoff as a result of albedo (AL), liquid water (LW) and stability option (ST) choices. The differences are calculated by as option 1 – option 0 for each process. Lines show mean differences, while ranges denote inter-annual variability. Monthly mean isotherm elevations for daily minimum, mean and maximum temperatures are also shown.

https://doi.org/10.5194/tc-2019-187
Preprint. Discussion started: 10 September 2019

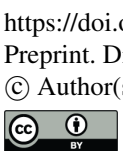

The Cryosphere Discussions
Open Access
EGU

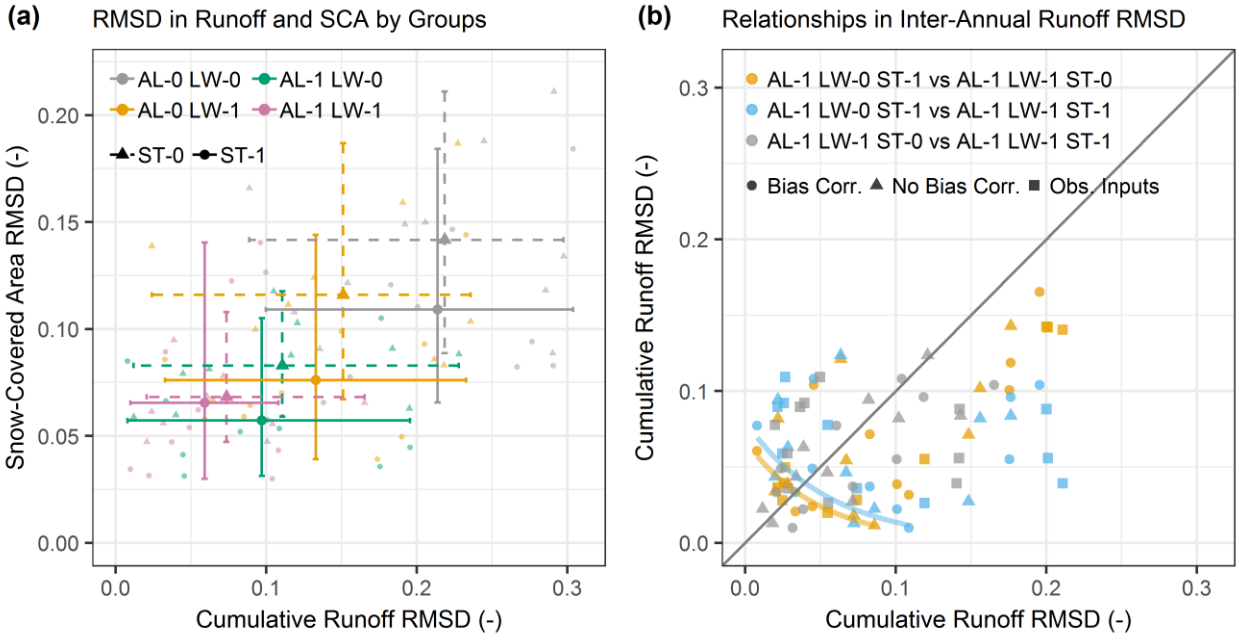

Figure 7. Inter-annual variation in model performance. Cumulative runoff RMSD is plotted against SCA RMSD in (a) for each of the albedo (AL) and liquid water (LW) option combinations (i.e. averaging respective ensemble members), with differentiation by stability (ST) option (shape and line type) also shown. Cumulative snowpack runoff RMSD is for the April to June period and normalised, whereas SCA RMSD is for April to September and based on an NDSI threshold of 0. In (b), the relationships between cumulative runoff RMSD for the three best-performing combinations are shown for each of the climate input strategies (see Section 3.2.3).

https://doi.org/10.5194/tc-2019-187
Preprint. Discussion started: 10 September 2019

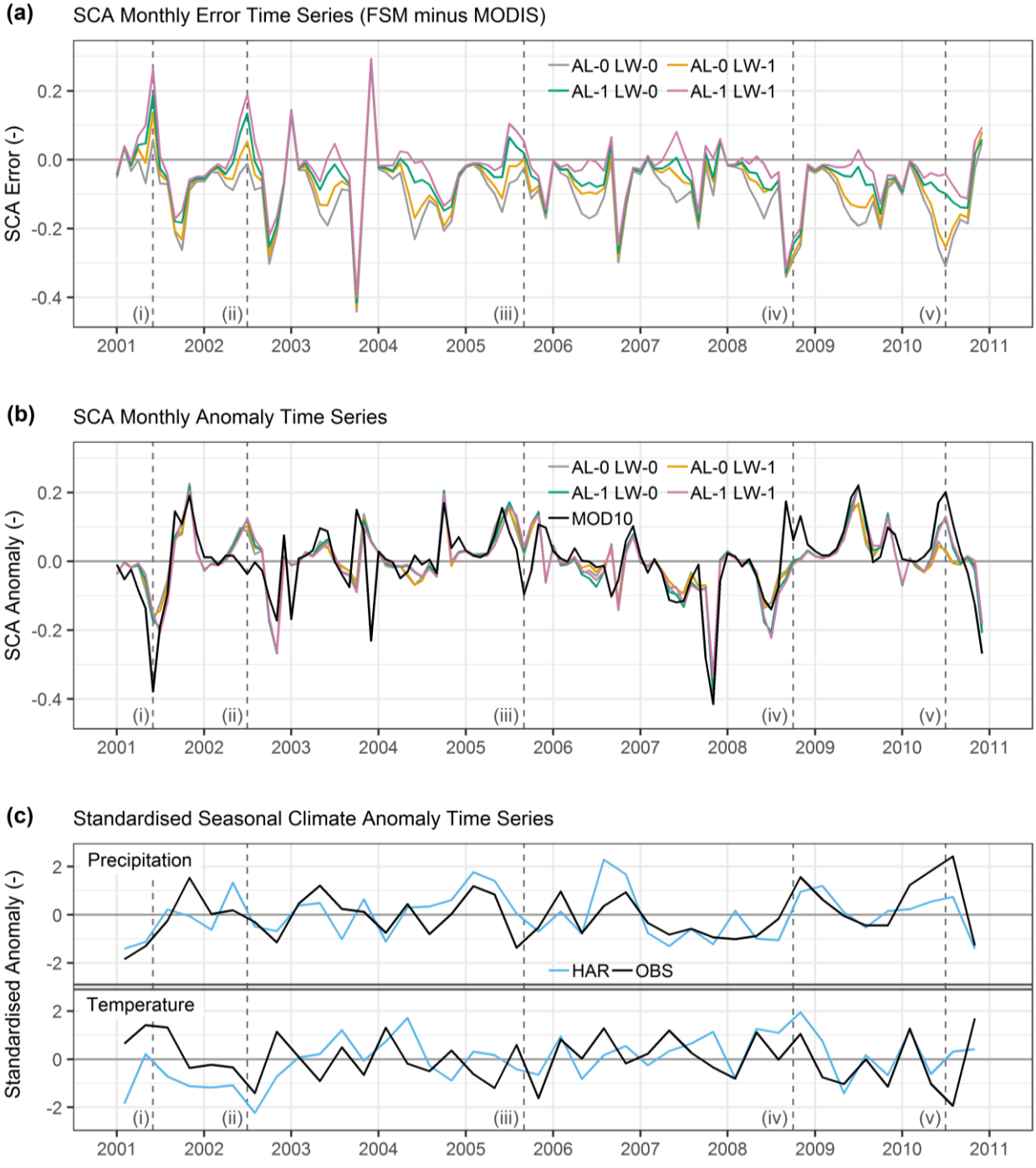

Figure 8. Comparison of model SCA performance in absolute and anomaly space with climate inputs. Monthly time series show (a) SCA errors relative to MOD10A1 (FSM minus MODIS) and (b) anomalies (subtracting monthly means from absolute SCA) after aggregating the ensemble by the combinations of albedo and liquid water parameterisations. Standardised seasonal precipitation and temperature anomalies based on observations aggregated from the climate stations in Figure 1b and the HAR are given in (c).

https://doi.org/10.5194/tc-2019-187
Preprint. Discussion started: 10 September 2019

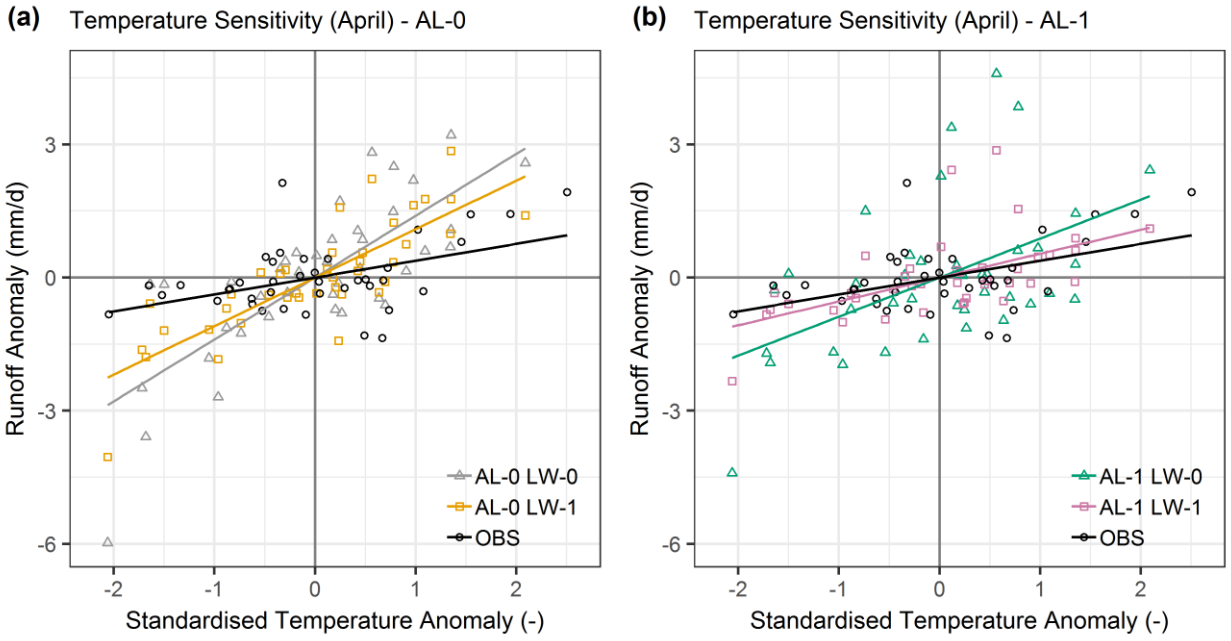

Figure 9. Sensitivity of simulated snowpack runoff (and observed total runoff) in April to temperature anomalies for combinations of albedo and liquid water process options (split across two panels for clarity). Points represent 10-day anomalies and lines are from linear regression.